THE EFFECTS OF CONDENSATION ON THE FLOW FIELD PROPERTIES IN FREE-JET EXPANSIONS OF ARGON

E. C. Ruby, R. F. Brown, and M. R. Busby

ARO, Inc.

August 1970

VON KÁRMÁN GAS DYNAMICS FACILITY
ARNOLD ENGINEERING DEVELOPMENT CENTER
AIR FORCE SYSTEMS COMMAND
ARNOLD AIR FORCE STATION, TENNESSEE

NOTICES

When U. S. Government drawings specifications, or other data are used for any purpose other than a definitely related Government procurement operation, the Government thereby incurs no responsibility nor any obligation whatsoever, and the fact that the Government may have formulated, furnished, or in any way supplied the said drawings, specifications, or other data, is not to be regarded by implication or otherwise, or in any manner licensing the holder or any other person or corporation, or conveying any rights or permission to manufacture, use, or sell any patented invention that may in any way be related thereto.

Qualified users may obtain copies of this report from the Defense Documentation Center.

References to named commercial products in this report are not to be considered in any sense as an endorsement of the product by the United States Air Force or the Government.

THE EFFECTS OF CONDENSATION ON THE FLOW FIELD PROPERTIES IN FREE-JET EXPANSIONS OF ARGON

E. C. Ruby, R. F. Brown, and M. R. Busby
ARO, Inc.

FOREWORD

The research reported herein was jointly sponsored by Headquarters, Arnold Engineering Development Center (AEDC), Air Force Systems Command (AFSC), Arnold Air Force Station, Tennessee, under Program Element 64719F, and AFCRL, L. G. Hanscom Field, Bedford, Massachusetts, under Program Element 6210lF.

The results of the research were obtained by ARO, Inc. (a subsidiary of Sverdrup & Parcel and Associates, Inc.), contract operator of AEDC, AFSC, under Contract No. F40600-71-C-0002. The work was performed under ARO Project No. SW5009 during the period from July 1969 to April 1970. The manuscript was submitted for publication on April 21, 1970.

The technical report has been reviewed and is approved.

Eules L. Hively
Research and Development Division
Directorate of Technology

Harry L. Maynard
Colonel, USAF
Director of Technology

ABSTRACT

Molecular beam techniques and a time-of-flight velocity distribution detector system were used to investigate the effects of condensation in free-jet expansions of argon. A 1-in.-diam skimmer cooled to 22°K was used to eliminate skimmer interaction. The data reported are for 170, 300, and 600°K argon expanded into a vacuum from source pressures of from 10 to 10,000 torr and with a nozzle-skimmer separation distance of 650 nozzle diameters. The data revealed that the mean velocity of the monomer species can be greater than predicted by $c_p T_o = \frac{1}{2} m v_m^2$ when condensation occurs. This is hypothesized to be the result of the heat of condensation being added to the flow field. Also, when condensation occurs, the static temperature increases. Terminal speed ratios as high as 27.5 were measured during these tests.

CONTENTS

APPENDIXES

NOMENCLATURE

b_o	Constant, $b_o = 2/3\ \pi\ N_o d^3$
C	Constant
c_p	Specific heat at constant pressure
D_n	Orifice diameter
d	Molecular diameter
F_r	Free energy of a drop of radius, r
F_∞	Free energy of a large liquid surface
f_r	Fugacity of a drop of radius, r, at gas and liquid phase interface
f_∞	Fugacity of a large liquid surface at gas and liquid phase interface
K	Initial relative kinetic energy or the total energy of a center of mass system
Kn_s	Knudsen number evaluated at the source
k	Boltzmann's constant
L	Flight length from chopper to detector
M	Mach number
M_K	Condensation Mach number
M_T	Terminal Mach number
m	Mass of a molecule
$\dot{N}$	Total beam flux
N_o	Avagodro's number
P	Pressure
P_B	Sum of pressures produced by beam and background gas
P_{BG}	Pressure of background gas in chamber
p_K	Actual pressure of condensation

p_o	Source pressure
p_r	Vapor pressure of a drop of radius, r
p_∞	Vapor pressure of a flat liquid surface
R	Gas constant
r	Molecular radius or molecular separation in Eqs. (8) and (9)
r^*	Critical radius of a drop which must be present for condensation to occur
$S_d(t)$	Signal distribution function
SR	Speed ratio
T	Temperature
T_K	Actual temperature of condensation
T_o	Source temperature
T_s	Static temperature
t	Time
t_c	Time delay between photoelectric trigger and beam molecules leaving chopper
t_D	Waveform eductor time delay
t_m	Time of maximum signal
t_o	Time associated with flow velocity, U_o
t_s	Spectrometer time delay—the time between beam ionization and detection
U	Centrifugal potential
U_o	Flow velocity of the beam
v	Thermal velocity
v_m	Velocity corresponding to the time of maximum signal
v_{mp}	Most probable velocity
W	Thermodynamic probability

X_{2B} Concentration of bound dimers

a Lower limit of molecular separation for which repulsive potential, $\phi(r)$, is zero

a_1 Beam flux gage calibration constant

β Constant $\beta = m/2kT$

γ Specific heat ratio

Δt "On" time of a single waveform eductor module

ϵ Total depth of potential well

λ_o Mean free path at source conditions

η Surface tension

ρ Density

ρ_L Density of liquid phase

ρ_o Density at source conditions

ϕ Gas supersaturation

ϕ_k Gas supersaturation at which condensation occurs

$\phi(r)$ Interaction potential

SECTION I
INTRODUCTION

In the normal theory of condensation in large-scale jets, the condensation line uniquely defines the pressure and temperature conditions which are necessary before a pure, neutral gas can condense. The normal theory is adequate if a small mean-free path exists between particles in an expanding jet since the interaction between particles results in a quasi-equilibrium condition.

With the advent of the space age, it has become apparent that the normal theory is inadequate for analyzing condensation effects in a free-jet expansion (i.e., expansion from high-pressure reservoir conditions into a near vacuum). The greater mean-free path between particles results in a much greater time rate associated with the condensation process, and the quasi-equilibrium assumptions are no longer valid.

A better understanding of condensation and molecular cluster formation in a free-jet expansion is needed. These phenomena are important considerations in space-related problems, such as determining

1. The gas dynamic characteristics of highly expanded rocket gas plumes from space propulsion systems,

2. The effect of the forces generated by molecular clusters when these clusters impinge on a body immersed in a rocket plume, and

3. The expansion characteristics of reactive gases such as nitrous oxide (NO) which are used in high altitude research.

An approach to analyzing the condensation phenomena in a free-jet expansion is to allow the expansion to proceed to its terminal Mach number, isolate the core of the expanded jet, and measure the velocity distribution of the different size molecular clusters in this core. The measurement of the relative abundances and velocity distributions of molecular clusters in the condensation region provides additional data which can be used in the analysis of the mechanism of condensation.

Concurrent developments in aerodynamic molecular beam technology and the theory of condensation in a free jet during the last two decades allow the approach outlined above to be used. These developments fall into three broad categories:

1. Improvements in distinguishing between the effects of the molecular beam and the background gas present in the molecular beam chamber,

2. The development of methods for analyzing time-of-flight (TOF) data and of obtaining simple moments (i.e., weighted integrals) based on information which is directly available in terms of TOF measurements, and

3. The development of a qualitatively valid model of the condensation process in a free jet.

Concurrent with the improvements in aerodynamic molecular beam technology, various investigators contributed bits and pieces of evidence which indicate that the formation of molecular clusters is an intrinsic part of the condensation process. The development of this theory is chronologically developed in the following paragraphs.

If a gas in a cloud chamber apparatus is expanded into a region of lower pressure, the degree of expansion required to achieve condensation is determined by the point of intersection of the pressure-temperature adiabat and the condensation line. The condensation line uniquely defines the pressure and temperature conditions under which a pure neutral gas will condense. Normally the gas does not condense when it reaches the saturated state, but instead it requires a certain degree of supersaturation to bring about droplet formation. If p_K and T_K are the actual pressure and temperature of condensation, the appropriate supersaturation, ϕ_K, is defined by p_K/p_∞ (Ref. 1).

The relationship between the fugacity of a drop in equilibrium with a gas over a spherical drop surface of radius, r, and the fugacity of a large liquid surface in equilibrium with the same gas can be expressed by

$$F_r - F_\infty = RT \ln \frac{f_r}{f_\infty} = \frac{2\eta v}{r} \tag{1}$$

as developed in Ref. 2.

For a perface gas, the ratio of vapor pressures and the fugacity ratio are identical. By substituting vapor pressures for fugacities and manipulating the equation, the Kelvin-Helmholtz equation is produced:

$$\ln \frac{p_r}{p_\infty} = \frac{2\eta}{r} \frac{m}{\rho_L kT} \tag{2}$$

where η is the surface tension, k is the Boltzmann constant, ρ_L is the liquid density, and m is the mass of the molecule.

Since the ratio, p_r/p_∞, is a measure of the supersaturation, ϕ, it follows from Eq. (2) that for every value of ϕ, there exists some radius, r, of liquid drops which would be just the right size to remain in equilibrium with the vapor.

When condensation actually does occur, then

$$\ln \frac{p_{r^*}}{p_\infty} = \ln \phi_k = \frac{2\eta}{r^*} \frac{m}{\rho_L kT} \tag{3}$$

The term, r^*, is defined as the "critical radius." This radius represents the minimum size of drop which must be present for condensation to occur.

The concept of a "critical radius" leads to the conclusion that a supersaturated vapor cannot condense until it contains certain "condensation nucleii." In 1897, Wilson suggested that a pure neutral gas at a sufficiently large value of ϕ would contain these nucleii in the form of small molecular clusters. Wilson postulated that intermolecular forces gave each molecular cluster a finite lifetime during which it could either grow by assimilation of further molecules or decay through evaporation. The size of the molecular cluster would determine which of the two processes was more probable. He further postulated that the probabilities of growth or decay must be equal for an assembly of critical size so that stable equilibrium with the vapor is established. This growth to a critical radius has come to be called "self-nucleation" and the sub-critical and critical assemblies are denoted as "condensation embryos" and "condensation nucleii," respectively.

The early cloud chamber research introduced the basic concept that for condensation to occur, an assembly of "critical radius" condensation embryos must be present. This idea proved valid in condensation studies of expanding jets under continuum flow conditions.

In a free-jet expansion, the greater mean-free path between particles results in a much greater time rate associated with the condensation process, and the quasi-equilibrium assumptions are no longer valid. The physics of the problem, however, would still lead to the belief that "critical radius" molecular clusters must exist somewhere in the free-jet flow field before droplet formation can occur.

Leckenby, et al. (Ref. 1), proposed that the formation of molecular clusters in a free jet was caused by a condensation process brought about by adiabatic cooling as the gas expanded from the source orifice. In the continuum region of the expansion, the gas gains linear kinetic energy at the expense of its enthalpy and accelerates to supersonic Mach numbers while the temperature, pressure, and density all decrease. The relationship between these parameters is given by the well-known equation:

$$\frac{T}{T_o} = \left[1 + \frac{1}{2}(\gamma - 1) M^2\right]^{-1} = \left(\frac{p}{p_o}\right)^{(\gamma-1)/\gamma} = \left(\frac{\rho}{\rho_o}\right)^{\gamma-1} \tag{4}$$

Leckenby expressed the line of a saturated vapor pressure curve as

$$\ell n\, p_\infty = A - B/T \tag{5}$$

where p_∞ is the vapor pressure over a flat surface, and A and B are constants for a particular vapor. The vapor does not condense on reaching the saturated state but requires a certain degree of supersaturation before droplet formation occurs. The appropriate supersaturation was previously defined as

$$\phi_k = \frac{p_k}{p_\infty} \tag{6}$$

Leckenby, therefore, expressed the equation of the condensation line by manipulating the equation for the saturated vapor line, Eq. (5), as follows:

$$\ell_n\left(\frac{p_k}{\phi_k}\right) = A - \frac{B}{T_k} \tag{7}$$

Equation (4) could now be used to determine the Mach number at the point of condensation:

$$\ell_n\left[\frac{p_o}{\phi_k}\left\{1 + \frac{1}{2}(\gamma - 1)M_k^2\right\}^{\frac{-\gamma}{\gamma-1}}\right] = A - \frac{B}{T_o}\left[1 + \frac{1}{2}(\gamma - 1)M_k^2\right] \tag{8}$$

Equation (8) implies that early condensation (i.e., small M_K) can be affected by increasing p_o, decreasing T_o, and using a gas with a large γ value.

Leckenby realized that a free-jet expansion involves a transition from continuum flow to free molecular flow during which the adiabatic cooling ceases, and after which temperature and flow velocity remain constant. The final temperature and flow velocity determine the terminal Mach number, M_T. He, therefore, established the condensation criteria that M_T must be greater than M_K before condensation conditions are possible.

Based on the relationships developed in Appendix II, Leckenby concluded that the terminal Mach number depends on the reservoir conditions (p_o, T_o) and γ in a directly contrary sense to the condensation Mach number, M_K. He concludes (Ref. 1) that "high reservoir pressures, low initial temperatures, and the use of a gas with a high γ are conducive to well-advanced expansions (large M_T) and early condensation (low M_K)."

Lenkenby also noted (Ref. 1) that the observation of molecular clusters is so closely tied to the expected occurrence of condensation in the gas "that it is difficult to avoid the inference that the one is a direct manifestation of the other. The results show that, in general, the clusters appear in greater abundance and at lower pressures for gases which have high critical temperatures (i.e., are easily liquified by cooling), except insofar as the expansion is modified by the variable γ."

The existence of dimers (two atoms bound together by van der Waals interaction) is well documented in the literature (Refs. 1, 3, 4, and 5).

Jeans (1904) envisioned the formation of dimers as resulting from three-body collisions in which the act of binding occurs when excess energy is removed by some third body.

Leckenby and Robbins (Ref. 1) proposed in 1965 that dimers are the smallest condensation embryos present in a gas. These dimers exist in all gases if the temperature is low enough for the attractive van der Waals interaction to be significant and when the pressure is high enough to produce a significant number of three-body collisions. The dimers exist independent of whether the gas is in a saturated or unsaturated condition.

Stogryn and Hirschfelder (Ref. 6) have shown that, at temperatures less than the critical temperature, the dominant contribution to the second virial coefficient is from bound dimers. They have computed that two types of dimers can exist: (1) bound dimers and (2) metastable dimers.

If an interaction potential, $\phi(r)$, is considered, it may be shown that, by applying Maxwell-Boltzmann statistics to the system of interacting atom pairs, the probability of finding a pair with separation between r and (r + dr) and with relative kinetic energy between U and (U + dU) is:

$$d^2W = A \exp\left[-\left(\frac{7 + \phi(r)}{kT}\right)\right] U^{1/2}\, dU\, r^2\, dr \tag{9}$$

where A is normalizing constant (Ref. 2).

Since the long range forces between molecules are attractive (Ref. 7), it follows that $\phi(r)$ is negative over a wide range of molecular separations. Hirschfelder, et al. (Ref. 8), concluded that, for certain pairs of atoms, the total energy U + $\phi(r)$ would be negative. This combination was defined as "bound" since, in the absence of external interactions, each atom is trapped in the potential well of its partner. The result of this type of bond is that the two atoms would orbit indefinitely about their common center of mass if no collisions occurred. In reality, the effect of collisions would soon result in the pair either: (1) absorbing enough energy from collisions to separate, or (2) capturing the colliding atom and forming a three-particle cluster. The occurrence of either event would be determined by the relative positions of the bound pair at the time of collision.

Stogryn, et al. (Ref. 6), calculated the concentration of bound dimers, X_{2B}, for a closed system in equilibrium based on the Lennard Jones potential:

$$\phi(r) = 4\epsilon\left[\left(\frac{a}{r}\right)^{12} - \left(\frac{a}{r}\right)^{6}\right] \tag{10}$$

where ϵ is the maximum depth of the potential well and a is the lower limit of r for which $\phi(r)$ is zero. They showed that

$$X_{2B} = \frac{1}{\sqrt{\pi}} \frac{b_o}{v_o} p \frac{273}{T} \left(\frac{4\epsilon}{kT}\right)^{3/2}\left[\frac{2}{3} \cdot \frac{2}{5} + \frac{2}{3} \cdot \frac{2}{5} \cdot \frac{2}{7} \cdot \frac{2}{9}\left(\frac{4\epsilon}{kT}\right)\right.$$

$$\left. + \frac{2}{3} \cdot \frac{2}{5} \cdot \frac{2}{7} \cdot \frac{2}{9} \cdot \frac{2}{11} \cdot \frac{2}{13} \cdot 21\left(\frac{4\epsilon}{kT}\right)^2 \cdots\right] \tag{11}$$

where

$$b_o = \frac{2}{3}\pi N_o d^3$$

v_o is the molar volume at standard conditions, and p is the pressure in atmospheres.

The essential features of Eq. (11) are that the concentration of bound dimers, X_{2B}, varied linearly with pressure and approximately as $T^{-5/2}$. It can also be concluded that gases with large attractive potentials (large ϵ) most readily form dimers.

Reference 6 notes that in addition to bound dimers which must meet the criterion of $(U + \phi(r))$ less than zero, another situation exists which can result in the formation of "metastable bound" dimers.

If $\phi(r)$ varies more rapidly than $1/r^2$, orbiting pairs may exist even if the total energy is positive. This situation results because the radial action of the interacting particle, when reduced to a one-dimensional problem, is governed by both the actual potential, $\phi(r)$, and the "centrifugal potential" which may be written Kb^2/r^2 where K is the initial relative kinetic energy and b is the impact parameter. The combination of $\phi(r)$ and the centrifugal potential (which is always positive) has a positive maximum somewhere in the attractive region of $\phi(r)$. The height and position of this maximum are determined by the parameters K and b as shown in Fig. 1 (Appendix I). A potential "ditch" exists between this "hump" and the repulsive part of $\phi(r)$ which confines the radial oscillations of any atom pair whose total energy is less than the hump height. These pairs fall into two classes, depending on whether their total energy is positive or negative.

Classical mechanics makes no distinction between pairs where

$$U + d(r) < 0 \qquad \text{(Bound dimer criterion)}$$

and

$$U + d(r) > 0 \qquad \text{(Metastable dimer condition)}$$

Leckenby, et al. (Ref. 1), points out that from the standpoint of wave mechanics, "pairs with positive energy (metastable dimers) are liable to disassociate by tunnel effect leakage through the hump."

Reference 6 gives a detailed treatment of bound and metastably bound dimers in gases. These results show that the fraction of metastably bound dimers is normally somewhat less than one-third of the total dimer abundance.

The central point to be made in this rather lengthy development is that theory leads to the recognition of two categories of dimers which both contribute significant amounts to the total dimer abundance. Classical statistical mechanics cannot distinguish between bound and metastably bound dimers. The metastably bound dimer, which has a positive total energy, would be assumed to have a greater tendency to disassociate upon collision, and it would also tend to have a higher average energy content.

In summary, aerodynamic molecular beam technology has progressed to the point where it can provide useful data about the condensation process in a free jet. The degree of correlation between these data and the existing free-jet condensation theory provides the "building blocks" which are necessary for a more complete understanding of the condensation process.

This investigation will experimentally determine the velocity distribution and relative abundances of the different mass number argon clusters in the condensation region of a free-jet expansion over a source pressure range of from 10 to 10,000 torr and source temperatures of 170, 300, and 600°K.

SECTION II
APPARATUS

2.1 AERODYNAMIC MOLECULAR BEAM SYSTEM

The AEDC aerodynamic molecular beam system (Fig. 2) is a stainless steel cylinder, 3 ft in diameter by 6-1/2 ft long, which is divided into three sections by two removable bulkheads. Vacuum conditions are produced and maintained in the cell by oil diffusion pumps, 20°K gaseous-helium-cooled cryoliners, and 77°K liquid-nitrogen-cooled cryoliners. The total pumping speed for air is in excess of 500,000 liters/sec. This system maintains pressures of 1×10^{-4}, 1×10^{-7}, and 3×10^{-8} torr in the nozzle discharge, collimation, and test sections of the chamber, respectively.

The apparatus used for generating the molecular beam during this series of tests consisted of a 4-mm-diam collimating orifice, a 2.54-cm-diam cryogenically cooled skimmer, a collimation distance of 44 cm a 0.34-mm-diam nozzle, and a nozzle-skimmer separation distance of 22 cm. A complete description of the beam system and its performance is given in Ref. 9.

2.2 BEAM SOURCE

Figure 3 depicts the tantalum tube, heat shield, and associated plumbing used as a variable temperature beam source. A resistance-heated tantalum tube, 8 in. long and 3/16 in. in diameter with a wall thickness of 0.01 in., was used to ensure high gas stagnation temperatures. The center of the tube contains a 0.014-in.-diam hole orifice. Additional metal was removed in the neighborhood of the orifice hole to ensure a thin-wall orifice nozzle. Large copper electrodes attached near the tube ends provided electrical power. A Chromel®-Alumel® thermocouple was welded directly to the tantalum in the vicinity of the orifice and was used to monitor source temperatures. A water-cooled copper heat shield surrounds the tantalum tube and serves to protect the cryopanels from the radiant heat emitted when the tantalum is used as a high temperature source. However, liquid nitrogen was circulated through the shield when a low temperature source was desired. All of the source temperature measurements were made with a thermocouple attached to the tube behind the orifice.

2.3 THE SKIMMER AND COLLIMATOR

A conical metal skimmer is commonly used during molecular beam experiments of this type. However, the results of previous investigations (Ref. 10) and an analysis of the flow field indicated that severe skimmer interactions may have occurred during many of the previous experiments conducted at AEDC and other laboratories. Therefore, the conventional skimmer was removed, and a copper "doughnut" cryocooled by gaseous helium (22°K) was used as a skimmer during the experiments.

Figure 4 depicts the cooled skimmer used during these tests. The skimmer is constructed of 1/8-in.-thick copper sheet. The orifice is a piece of 1-in.-diam copper tubing 1-3/4 in. in length. The outside diameter of the skimmer was tailored to fit the hole produced by removing the conventional skimmer. The skimmer outside diameter is approximately 8-1/2 in.

At low flow rates, a capture coefficient greater than 0.99 for argon on a 22°K argon cryofrost is reported in Ref. 11. The effects of high flow rates and changes in cryofrost crystallographic structure on the capture coefficient were unknown. An RF antenna was installed 3 in. in front of the skimmer face and used as a flow field visualization device so that the capture ability of the skimmer and degree of skimmer interaction could be qualitatively evaluated. Figure 5 depicts a region of high density in the flow field around the skimmer at room temperature (no cryocooling). Once the flow of gaseous helium was established and an initial argon cryofrost developed, this high density region completely disappeared.

2.4 THE DETECTOR SYSTEMS

The measurement of relative abundances of molecular clusters and the measurement of time-of-flight (TOF) data require different types of detector systems. Each detector configuration is discussed below.

2.4.1 The Total Flux Detector System

Total incident beam flux was measured with a miniaturized ionization gage mounted on a probe. This gage could be accurately positioned in the flow field. The gage was enclosed in the standard glass envelope, but the normal 1-in.-diam opening was reduced to 6 mm as shown in Fig. 6. Reducing the opening served to increase the sensitivity of the gage to directed gas flows and also ensured that molecular clusters were broken up by wall collisions so that a gage response could be obtained before the molecules escaped.

The total beam flux was obtained from

$$\dot{N} = a_1 (P_B - P_{BG})$$

where P_B is the measured beam pressure and P_{BG} is the measured background pressure. The calibration constant, a_1 (2.5×10^{20} molecules/sec torr for argon), was obtained by using an oven-type molecular beam to provide a known beam flux.

2.4.2 The Modulated Beam Detector

The modulated beam detection system used consisted of (1) a mechanical beam chopper, (2) a quadrupole mass spectrometer (2 to 600 amu), and (3) a lock-in amplifier Figure 7 indicates schematically the interconnection of these components.

The collimated molecular beam is chopped into pulses by two slots in a rotating wheel. These slots are 90-deg sectors cut out of a 2-in.-diam disc. The beam chopper is driven by a small two-phase synchronous vacuum rated motor generally turning at 40 Hz. These beam pulses then "fly-thru" the ionization region of a mass spectrometer, and an ionized sample of the beam is electronically deflected through the quadrupole section which is tuned to the mass number of the beam molecules. The resulting ion current is amplified by an electron multiplier which sends a pulsed electrical signal to the "lock-in" amplifier. This amplifier operates as a bandpass amplifier, centered on the chopper frequency. A light and photocell mounted at the chopper wheel provide the chopping frequency to the amplifier and keep it synchronized with the actual molecular beam modulation frequency. The lock-in amplifier increases the signal-to-noise ratio by amplifying only the proper frequency and phase with respect to the reference signal from the photocell. The amplifier signal is displayed on an oscilloscope, on a chart recorder, and on a voltmeter which is an internal part of the amplifier. Very detailed explanations of this particular detection system are contained in Refs. 9 and 12.

2.4.3 The Velocity Distribution Detection System

Reference 13 provides a detailed description of the detection system used to measure velocity distributions. A summary of the material developed in the cited reference follows.

The detection system was configured as illustrated in Fig. 7. The collimated molecular beam passes through the narrow slits of a chopper wheel which has been designed to provide an approximate impulse of molecules (Ref. 13).

As time elapses, the molecules spread according to their velocity distribution. The beam then passes through a focusing aperture plate which reduces the beam diameter to a size smaller than that of the smallest ionizer aperture. The spectrometer is operated as a flow density detector and measures the local particle density in the ion source as a time dependent function. The local density in the ion source is directly proportional to the arrival rate of the molecules and inversely proportional to their velocity.

The quadrupole section is tuned to the particular mass number of interest, and the resulting ion current is amplified by the electron multiplier. Essential to the operation of this system is a Field Effect Transistor (FET) emitter follower. The FET emitter follower acts as a buffer or impedance matching device between the required high amplifier input impedance at the electron multiplier output and the low impedance required for the coaxial cables which lead out of the chamber. Signal losses are minimized by mounting the FET emitter follower circuit directly on the quadrupole tube inside the vacuum chamber.

The spectrometer signal is given a time reference by means of the photoelectric cell arrangement shown in Fig. 8. A synchronous pulse referenced to chopper open time is added to the spectrometer signal in the differential preamplifier. This composite signal represents the molecular arrival rate which is time dependent referenced to a particular "start time" which is the time the chopper shutter opens plus the random noise of the background gas. The signal is then processed in the waveform eductor, a schematic of which is shown in Fig. 9.

Figure 9 traces the path of the incoming signal through the waveform eductor. The incoming composite signal is fed through one of several resistors onto a signal bus common to a memory bank of 100 capacitors. These capacitors are connected to the signal bus by means of an insulated gate-type FET. A precision oscillator acts as a clock and advances a ring counter which controls the memory gates. This oscillator, which is an internal part of the waveform eductor, is externally triggered by the chopper synchronous pulse. The effect of this circuitry is to allow each of the 100 capacitors to be connected for consecutive equal time periods to the signal bus. By synchronizing this switching action with the chopper and the flight time of the gated molecular beam, the same portion of the velocity distribution is applied to any given capacitor on successive sweeps. Since the signal is being integrated as a result of the selected time constant, the noise is suppressed. The capacitors are also connected to a high input impedance amplifier which effectively isolates them from the output terminations. The memory can be erased or read out at a speed which is compatible with the data recording equipment used. The readout speed is independent of the speed used to store data.

The waveform eductor was connected to three output devices:

1. An oscilloscope which was used to monitor data acquisition,
2. An X-Y plotter which served to maintain a permanent record of the experiments, and
3. A data logger that provided a punched tape which was used as a computer input for data reduction purposes.

SECTION III
EXPERIMENTAL PROCEDURES AND FACTORS AFFECTING THE DATA

3.1 INTRODUCTION

Two separate sets of experiments were conducted. Initially, the concentrations[1] of the monomer, dimer, and trimer molecular clusters were determined as plots of source pressure versus signal strength for source temperatures of 170, 300, and 600°K. Velocity distribution measurements were made at various source pressures and temperatures and the flow field properties (most probable velocity, static temperature, speed ratio, etc.) were determined.

3.2 SOURCE CONDITIONS

A source to skimmer entrance distance of 22.2 cm was used for all of the experiments. Calculations indicate that this separation distance will ensure free molecular flow through the detector over the range of experimental conditions.

---

[1]Concentrations refer here to the actual mass spectrometer signal obtained for each polymer at various source conditions.

All values of p_o were measured with calibrated aneroid-type dial gages. From 0 to 800 torr, an accuracy of ±1 torr was obtained with the gage used. In the range from 800 to 5000 torr, an accuracy of ±10 torr was obtained with a Kollsman gage. Above 5000 torr, accuracy was considerably reduced, and the margin of error is estimated as ±500 torr for this gage.

A Chromel-Alumel thermocouple was welded to the outer wall of the tantalum source opposite the source orifice. Previous experimental results had shown that the temperature of the outer wall of the thin wall (0.010 in.) tantalum tube would be essentially the same as the stagnation temperature, T_o, of the gas in the tube.

The experimental conditions and procedures used in each of the two sets of experiments are developed separately below.

3.3 MEASUREMENT OF THE CONCENTRATIONS OF MOLECULAR CLUSTERS

These measurements were conducted using experimental procedures developed during previous AEDC tests (Ref. 14). A summary of these procedures is as follows.

The total beam flux versus p_o was measured using the miniaturized ionization gage discussed in Section 2.4.1.

The modulated beam detection system was used to measure the concentrations of the various size molecular clusters at source stagnation temperatures of 170, 300, and 600° K. All external spectrometer controls were optimized and held constant during the measurements. The mass spectrometer was initially tuned to argon mass 40. The spectrometer signal was recorded as the source pressure was incrementally increased. Successively higher mass number signals were recorded by tuning the spectrometer to the new mass number and incrementally traversing the source pressure in alternate directions (i.e., one set of data was taken with the source pressure varying from high pressure to low pressure and the next set was taken with source pressure varying from low to high). After taking the measurements, mass 40 was remeasured to determine if the mass spectrometer sensitivity had changed during the test.

The higher mass number molecular clusters required fairly high beam intensities in order to properly phase the lock-in amplifiers. Lock-in was accomplished by:

1. Raising the source pressure until a visible signal was detectable on the oscilloscope,

2. Adjusting the detector system to respond to the species of interest, and

3. Incrementing the source pressure over the desired range and recording the mass spectrometer signal.

3.4 FACTORS AFFECTING THE DATA

Interpretation of the quadrupole mass spectrometer signal in terms other than relative signal strength involves a great many variables which are not all well understood at this time. Since the purpose of the molecular cluster concentration measurements was to determine the source pressures and temperatures at which the various mass number molecular clusters attained a maximum value, signal strength serves as an adequate measurement parameter.

In Refs. 3 and 14 are discussed inherent errors and unknowns in the use of mass spectrometers. Those areas of mass spectrometry which influenced the experiment are discussed below.

The ionization cross section of argon molecular clusters is unknown. Previous investigators assumed that the field of interaction for an electron is small with respect to the diameter of an argon atom and that an electron would have an ionization probability for a molecular cluster equal to the sum of the ionization probabilities for the atoms in the cluster (Ref. 14).

The possible effect of cluster fragmentation due to the ionization process in the mass spectrometer is also difficult to assess. During these experiments, the ionizing electron energy was varied from 20 to 90 ev, and the relative concentrations of the molecular clusters did not change with electron energies less than 60 ev.

The electron multiplier sensitivity is a function of the age and environment of the multiplier unit. A new electron multiplier has maximum sensitivity during about the first eight hours of use. This initial eight hour period is also the time when its sensitivity decreases at the greatest rate. A new electron multiplier was installed in the mass spectrometer at the start of the molecular cluster concentration measurements. The new multiplier ensured optimum sensitivity at the expense of repeatability. A recheck of data points at the conclusion of each experiment produced good repeatability but overall spectrometer sensitivity decreased by approximately 10 percent during the course of the experiment.

In summary, the goal of this series of experiments was to determine the source pressures at which the various size molecular clusters achieved maximum signal values. With this objective in mind, it seems reasonable to measure concentrations in terms of uncorrected spectrometer readings.

3.5 MEASUREMENT OF THE VELOCITY DISTRIBUTION OF MOLECULAR CLUSTERS

The velocity distribution detection system was installed as shown in Fig. 8, and the pressure and temperature of the source were controlled in the same manner as before.

Initial phasing of the detection system was accomplished by operating at a fairly high source pressure and tuning the quadrupole section of the spectrometer to the desired

molecular cluster mass number. This high intensity signal could be monitored on the oscilloscope and readily identified by its chopped appearance.

After phasing was completed, the source pressure was reduced and TOF measurements were made over the range of source pressures and temperatures by the following procedure:

1. The source pressure and temperature were stabilized at desired values and the miniaturized ionization gage was raised out of the path of the molecular beam.

2. The waveform eductor was operated in analyze mode with a 20-sec time constant.

3. The signal storage of the waveform eductor was monitored on an oscilloscope and sufficient time (30 to 40 sec) was allowed to ensure complete signal storage in the eductor. This complete signal storage was attained when no further signal increase could be detected with the oscilloscope operated in an expanded range.

4. The eductor was then operated in readout mode, and an X-Y plot and a data log tape of the stored signal were obtained.

5. The miniaturized ionization gage (Fig. 6) was lowered into the path of the molecular beam thus turning the beam "off."

6. The background-signal was stored in the eductor and then read out on the X-Y plotter and the data tape. This background signal (beam-off signal) established the base line reference for each eductor module.

Details pertinent to TOF analysis are included in Ref. 13. The computer program used to process the data tape is discussed in Ref. 15.

The functions of the signal distribution, $S_d(t)$, computed from the data are affected by four factors:

1. Accuracy of the flight length, L, measurement,

2. Accuracy of the time measurements,

3. Gas purity, and

4. The agreement of the fit between the experimental signal distribution and the analytical expression:

$$S_d(t) = Ct^{-4} \exp\left[-\beta^2 L^2 \left(\frac{1}{t} - \frac{1}{t_o}\right)^2\right] \tag{12}$$

which is derived in Ref. 15.

Each of the four factors is discussed in turn below.

3.5.1 Accuracy of the Flight Length, L, Measurement

To minimize the effects of flight distance error, it is desirable that the flight distance be as long as possible within the physical constraints of the molecular beam chamber. Initially, a flight distance, L, of 30.2 cm was used. During later experiments, this distance was increased to 33.5 cm by an improved chopper mounting technique. The accuracy of the flight distance measurement is estimated to be ±0.05 cm.

3.5.2 Accuracy of the Time Measurements

The time measurements are each subject to different degrees of error:

1. The time delay between the photoelectric trigger and the pulse of molecules leaving the chopper, t_c, was obtained by comparing the light pulse and chopped beam signals on separate traces of the oscilloscope. This measurement was made to an accuracy of one microsecond, and its error is considered negligible.

2. The time delay between ionization and signal detection, t_s, was measured by using a precision 5-μsec pulse generator to gate the ion beam at the focus aperture of the mass spectrometer. The 5-μsec pulse and the detected signal were compared on separate traces of the oscilloscope, and this time delay error is considered negligible.

3. The time delay between the photoelectric trigger and the "turn-on" of the first eductor module, t_D, is controlled by a precision potentiometer which is calibrated in 1-μsec increments. Calibration of this control against a crystal reference standard showed a maximum error of 2 μsec when time delays in the 500-μsec range were used. A 500-μsec time delay is a typical time delay used in the experiments, and this error is considered negligible.

4. The sweep duration of the waveform eductor, 100 Δt, has the least precision of any of the time factors discussed. The waveform eductor sweep duration dial setting is calibrated in 50-μsec increments, and it is possible to misalign the dial by ±5 μsec even if it were in perfect calibration. When calibration error is included, this time can be in error by as much as ±10 μsec.

3.5.3 Gas Purity

All bottles were certified as at least 99.995-percent pure. However, one set of data was discarded because chemical analysis of the contents of one gas bottle revealed gas impurities. After this experience, the contents of each bottle of argon were analyzed by traversing the signal spectrum of the mass spectrometer.

3.5.4 Agreement between the Experimental and Theoretical TOF Distributions

The single factor which has an overwhelming effect on the data is the quality of fit between the analytical function and the observed data. All of the values determined by TOF analysis are functions of the analytical expression, Eq. (12), which is fitted by the least-squares technique to the experimental data. The velocity at which maximum signal occurs, v_m, can be determined with a high degree of repeatability since by definition:

$$v_m = \frac{l}{t_m} = \frac{\text{Flight Distance}}{\text{Time of Maximum Signal}}$$

The parameter, v_m, is least influenced by the quality of the fit since it is dependent only on those data points in the immediate vicinity of the point of maximum signal (Ref. 15). The speed ratio, SR, on the other hand, depends on all the data points in the distribution curve (Appendix II) and is thus more sensitive to variations in the signal.

SECTION IV
THE EXPERIMENTAL RESULTS

The results presented in this section are representative of molecular cluster concentration data and of more than 350 TOF measurements. The polymer concentration data are discussed first and then the properties (most probable velocity, static temperature, and speed ratio) of the free-jet flow field.

4.1 CLUSTER CONCENTRATION DATA

Figures 10, 11, and 12 denote the relative signal strength produced by the molecular clusters as a function of source pressure (10 to 10,000 torr) for various source temperatures (170, 300, and 600°K). The total beam flux in each case was fitted to the mass 40 concentration curve in the region where no dimers were detected.

In a free-jet expansion of argon through a small nozzle (0.014-in.-diam), three basic processes occur as the source pressure is varied from 10 to 10,000 torr for a constant source temperature. First a rapid increase in the dimer concentration is observed. The local maximum in the dimer concentration curve occurs at successively higher pressures (90, 1500, and 6000 torr) as the source temperature is increased (170, 300, and 600°K, respectively) as shown in Figs. 10, 11, and 12. Second, stable low mass unit polymers (e.g. 120 AMU) appear and then concentration increases very rapidly with increasing source pressure. The local maxima in the polymer peaks also occur at higher pressures as the source temperature is increased. The low mass unit polymers decrease as classical condensation begins. However, in Figs. 10 and 11, the mass 80 and 120 concentration curves begin to increase for increasing source pressures after the onset of classical condensation.

4.2 FLOW FIELD PROPERTIES

The flow field properties, i.e. the velocity corresponding to the time of maximum signal, v_m, the static temperature, T_s, and speed ratio, SR, obtained from the TOF measurements are presented in Figs. 13, 14, and 15 as a function of source pressure for various stagnation temperatures.

4.2.1 The Velocity Corresponding to the Time of Maximum Signal

The velocity corresponding to the time of maximum signal, v_m, is the most accurately determined experimental flow field property and is defined as

$$v_m = \frac{L}{t_m}$$

where L is the flight distance and t_m is the time of the TOF maximum signal. For aerodynamic molecular beams, i.e., high-speed ratio beams, v_m is approximately the mean velocity of the flow field (Ref. 15). In Fig. 13a, v_m for both mass 40 and 80 continually increases as P_o increases for a stagnation temperature of 170°K. However, as shown in Fig. 14a, v_m for the mass 40 signal at T_o = 300°K increases abruptly at a source pressure of about 900 torr and then shows only a very slight increase with increasing source pressure beyond 1800 torr. The v_m for the mass 80 and 120 clusters is less than that of mass 40, but a slight increase with increasing p_o was observed.

The energy equation for a perfect gas expanded as a free jet to very small static temperatures is closely approximated by

$$c_p T_o = \frac{1}{2} m v_m^2$$

For a source temperature of 300°K, the stream velocity for a free jet of argon is 5.5 x 10^4 cm/sec. As shown in Fig. 14a, the measured v_m is approximately 5.45 x 10^4 cm/sec, and when condensation occurs, the value increases to approximately 6.2 x 10^4 cm/sec. On a macroscopic scale the increase in the mass 40 v_m at approximately 900 torr is possibly the result of the latent heat of condensation. Based on this hypothesis, one theorizes that the static temperature would increase (Fig. 14b) when the latent heat of condensation is added to the flow field. Thus, more molecular collisions would occur in the expansion. The result is that the lower molecular weight particles (i.e., mass 40) are accelerated. The exact collision, condensation, and evaporation processes that occur are not completely understood but the preceding provides a hypothetical macroscopic model of the general processes.

Figure 15a presents the velocities for mass 40, 80, and 120 as a function of source pressure at T_o = 600°K. The velocities for all mass numbers were observed to decrease as p_o was increased from 400 to 6000 torr. However, beyond 6000 torr (the p_o corresponding to the onset of massive condensation in Fig. 12), v_m for mass 40 began to level out and finally slightly increase at 10,000 torr. Unfortunately, the vacuum system would not allow increasing p_o beyond 10,000 torr, and thus the existence of the rise observed in v_m at lower temperatures was not able to be ascertained.

4.2.2 The Static Temperature

The static temperature of the flow field is determined by using a least-square technique (Ref. 15) to curve fit the data to a modified Maxwellian velocity distribution function, and then the corresponding temperature is calculated. Representative T_s data for source temperatures of 170, 300, and 600°K are presented in Figs. 13b, 14b, and 15b. For all cases, the static temperature at first decreases with increasing source pressure to a minimum (below 1°K for T_o = 170 and 300°K). Then appreciable condensation begins, and the heat of condensation is released into the flow field. The result is a rapid increase in the static temperature with increasing source pressures.

The static temperature data are the least accurate data presented because a small error in curve fitting can result in an appreciable error in the value of T_s. However, the general trends are repeatable over all source conditions.

4.2.3 The Speed Ratio

The speed ratio, SR, is defined as $U_o/\sqrt{2RT_s}$ and was obtained from the velocity distribution data as discussed in Ref. 15. The data for various values of T_o are shown in Figs. 13c, 14c, and 15c. All of the data exhibit the same trends, i.e., at first (as p_o increases) there is an increase in SR to a maximum value and then there is an abrupt decrease with increasing source pressure. This decrease could be due to the higher static temperatures that seem to be associated with the onset of classical condensation (Figs. 13b, 14b, and 15b).

The maximum speed ratio of 27.5 obtained for a T_o = 300°K and p_o = 400 torr (Fig. 14c) is greater than the maximum predicted by Scott, et al. (Ref. 16), and Hagena, et al. (Ref 17). Condensation does decrease the speed ratio as predicted (Ref. 16), but the decrease occurs only where appreciable condensation is present. Skimmer interaction has been virtually eliminated by cryogenic cooling in these tests. This experimental condition perhaps accounts for the fact that the measured speed ratios are higher than those observed during previous experiments by other investigators (Refs. 16 and 17).

SECTION V
CONCLUSIONS

This series of tests has established the following:

1. Condensation does occur in free-jet expansions, and it does affect the properties of the flow field.

2. Condensation tends to increase the mean velocities of the mass 40 species free-jet expansions.

3. The static temperature increases when appreciable condensation occurs.

4. Static temperatures lower than 1°K can be achieved in free-jet expansions of argon.

5. When massive condensation occurs, the speed ratio is greatly reduced.

REFERENCES

1. Leckenby, R. E., Robbins, E. U., and Trevalion, P. A. "Condensation Embryos in an Expanding Gas Beam " Proceedings of the Royal Society of London, Vol. 280, Series A, March 1964, pp. 409–429.

2. Lewis, G. N. and Randall, M. Thermodynamics. McGraw-Hill Book Company, Inc., New York, 1923.

3. Milne, T. A. and Green, F. T. "Mass Spectrometric Observations of Argon Clusters in Nozzle Beams." Midwest Research Institute Summary Technical Report, Kansas City, Missouri, August 1966.

4. Good, R.E., Golomb, D., DelGreco, F. P., Hill, D. W., and Whitfield, D. L. "Clusters in Nitric Oxide Jet Expansion." Paper presented at the Sixth International Symposium on Rarefied Gas Dynamics, Massachusetts Institute of Technology, Cambridge, Massachusetts, July 1968.

5. Milne, T. A. and Green, F. T. "Mass Spectrometric Study of Homogeneous Nucleation in Free Jets." Midwest Research Institute Summary Technical Report, Kansas City, Missouri (AD655292), July 1967.

6. Stogryn, D. E. and Hirshfelder, J. O. "Contribution of Bound, Metastable, and Free Molecules to the Second Virial Coefficient and Some Properties of Double Molecules." Journal of Chemical Physics, Vol. XXXI, 1959, pp. 1531–1545.

7. Lee, J. F., Sears, F. W. and Turcotte, D. L. Statistical Thermodynamics. Addison-Wesley Publishing Company, Reading, Massachusetts, 1963.

8. Hirschfelder, J. O., Curtiss, C. F., and Bird, R. B. Molecular Theory of Gases and Liquids. John Wiley and Sons, Inc., New Yrok, 1954. p. 168.

9. Brown, R. F. and Heald, J. H., Jr. "Description and Performance of a Molecular Beam Chamber Used for Cryopumping and Adsorption Pumping Studies." AEDC-TR-66-135 (AD641388), October 1966.

10. Brown, R. F. and Heald, J. H., Jr. "Background Gas Scattering and Skimmer Interaction Studies Using a Cryogenically Pumped Molecular Beam Generator." Rarefied Gas Dynamics Fifth Symposium. C.L. Brundin, ed., Academic Press, Inc., New York, 1967, pp. 1407–1424.

11. Busby, M. R. and Brown, R. F. "Preliminary Investigation of the Interaction of 0.30- to 0.54-EV Gaseous Argon with a Solid Argon Surface." AEDC-TR-69-195 (AD696106), November 1969.

12. Heald, J. H., Jr. "The Performance of a Mass Spectrometric Modulated Beam Detector for Gas-Surface Interaction Measurements." Vacuum, Vol. 17. September 1966, pp. 511–515.

13. Powell, H. M. and Heald, J. H., Jr. "A System for the Measurement of Velocity Distributions of Molecular Beams." AEDC-TR-68-151 (AD675306), September 1968.

14. Golomb, D., Good, R. E., and Brown, R. F. "Dimers and Clusters in Free Jets of Argon and Nitric Oxide." Journal of Chemical Physics, Vol. 52, 1970, p. 1545.

15. Ruby, E. C. "An Experimental Study of the Velocity Distribution and Relative Abundances of Argon Molecular Clusters in the Condensation Regions of a Free Jet." University of Tennessee Master's Thesis, December 1969.

16. Scott, J. E., Jr. and Phipps, J. A. "Translational Freezing in Freely Expanding Jets." in Rarefied Gas Dynamics Fifth Symposium, Vol. II, C. L. Brundin, ed., Academic Press, Inc., New York, 1967, pp. 1337–1352.

17. Hagena, O. F. and Morton, H. S., Jr. "Analysis of Intensity and Speed Distribution of a Molecular Beam From a Nozzle Source." in Rarefied Gas Dynamics Fifth Symposium Vol. II, C. L. Brundin ed., Academic Press, Inc., New York, 1967, pp. 1369–1384.

18. Anderson, J. B., Andres, R. P., and Fenn, J. B. "Supersonic Nozzle Beams." Advances in Chemical Physics, J. Ross, ed., Vol. 10, John Wiley and Sons, Inc., New York, 1966, pp. 275–318.

APPENDIXES

I. ILLUSTRATIONS
II. THE SPEED RATIO

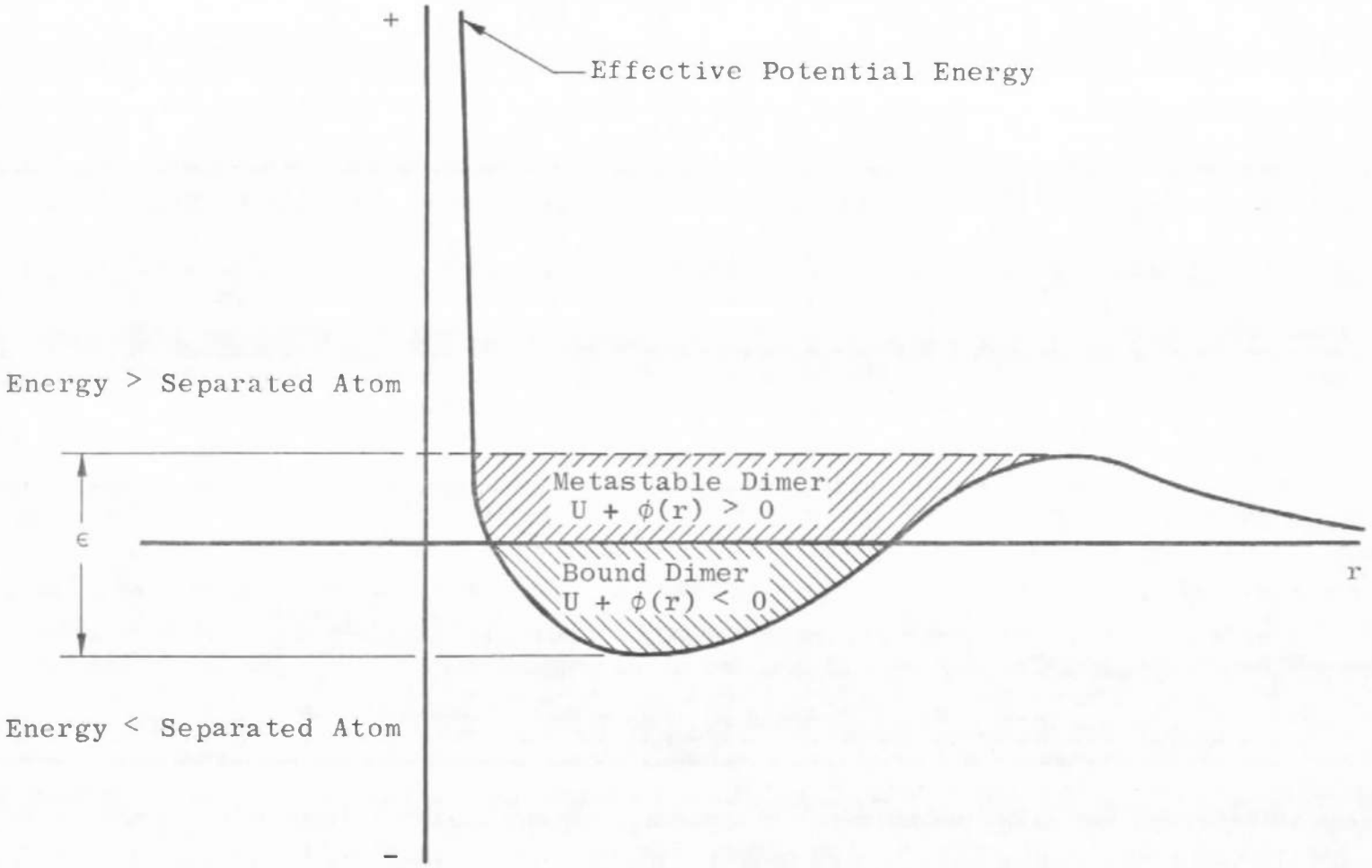

Fig. 1 Effective Potential Energy of Bound and Metastable Dimers

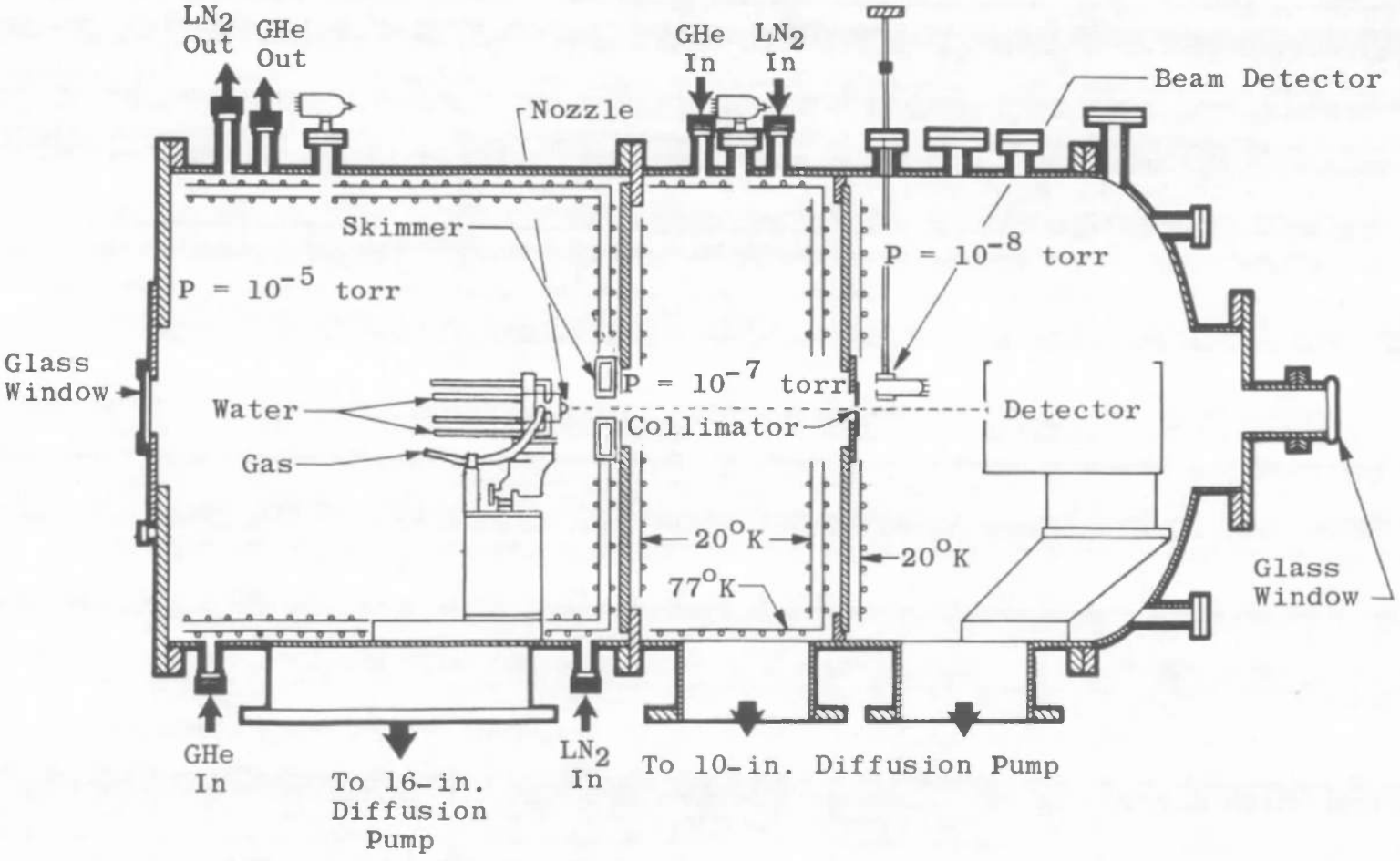

Fig. 2. The Molecular Beam Chamber

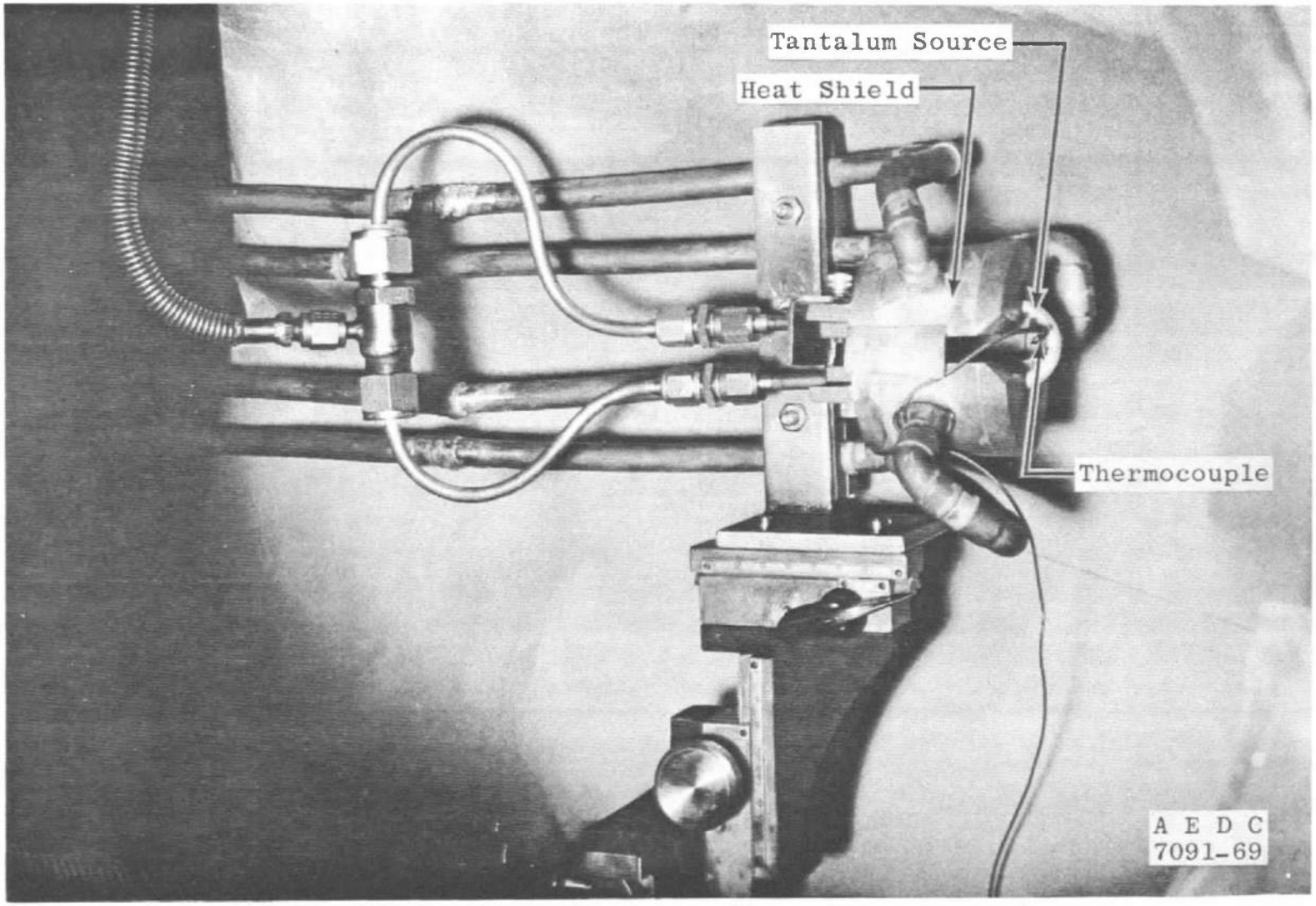

Fig. 3 Photograph of the High Temperature Beam Source

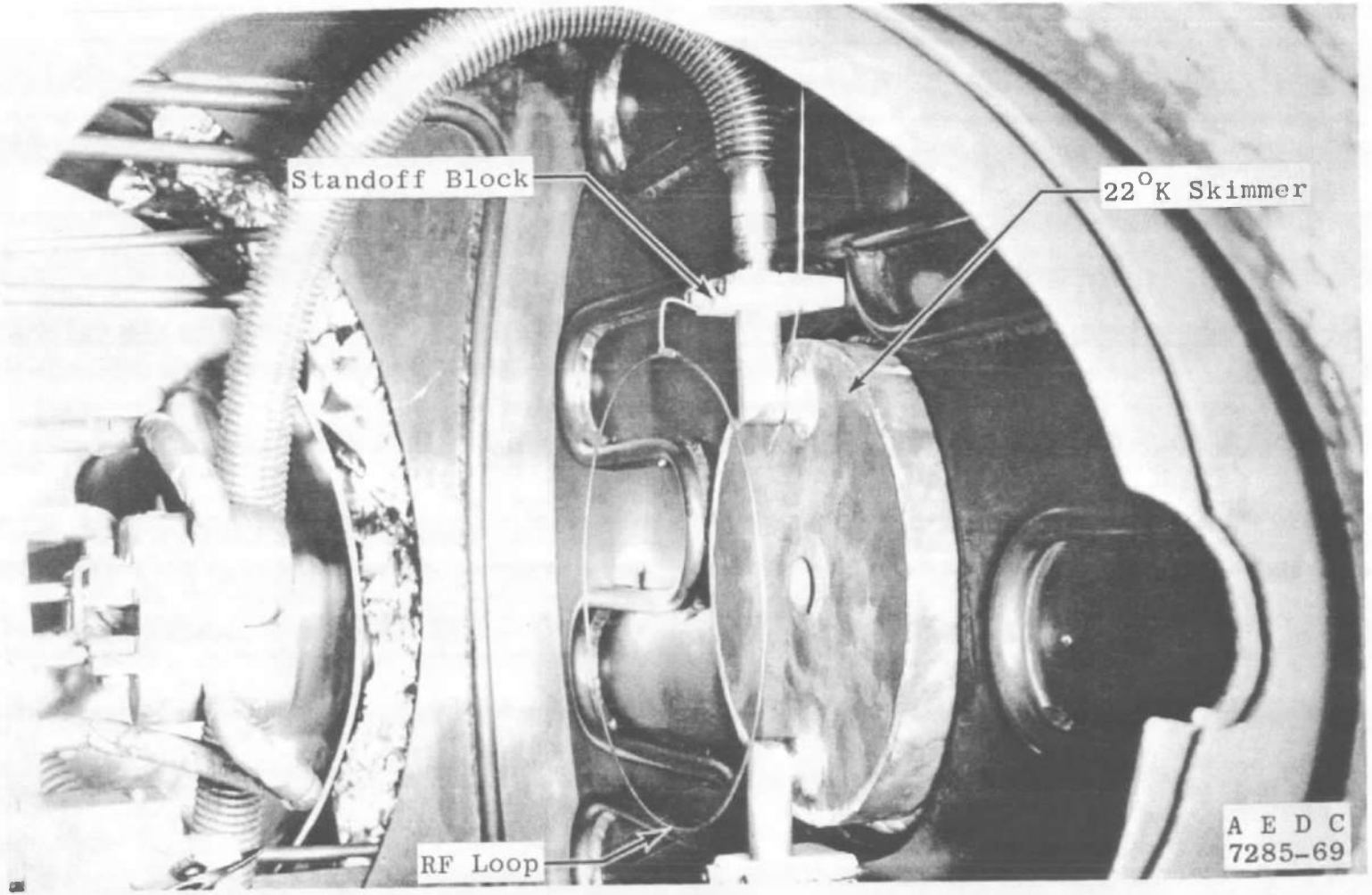

Fig. 4 Photograph of the Gaseous-Helium-Cooled Skimmer

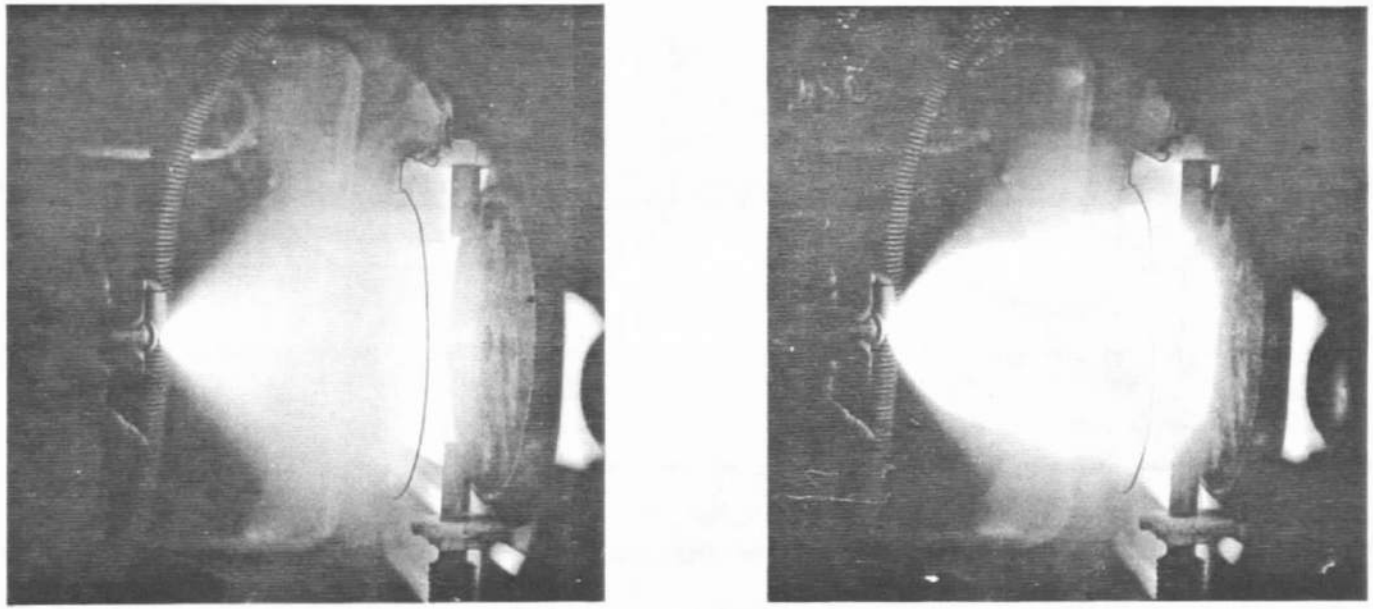

p_o = 725 torr

p_o = 1270 torr

T_o = 300°K

Fig. 5 Flow Field around the Uncooled Skimmer

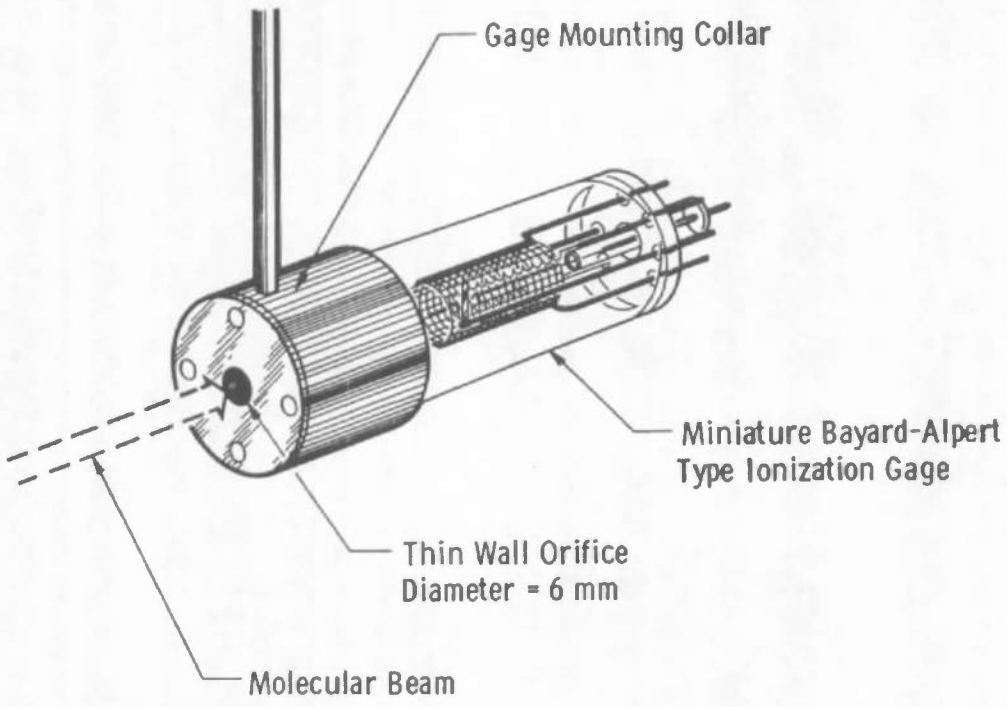

Fig. 6 Total Incident Beam Flux Gage

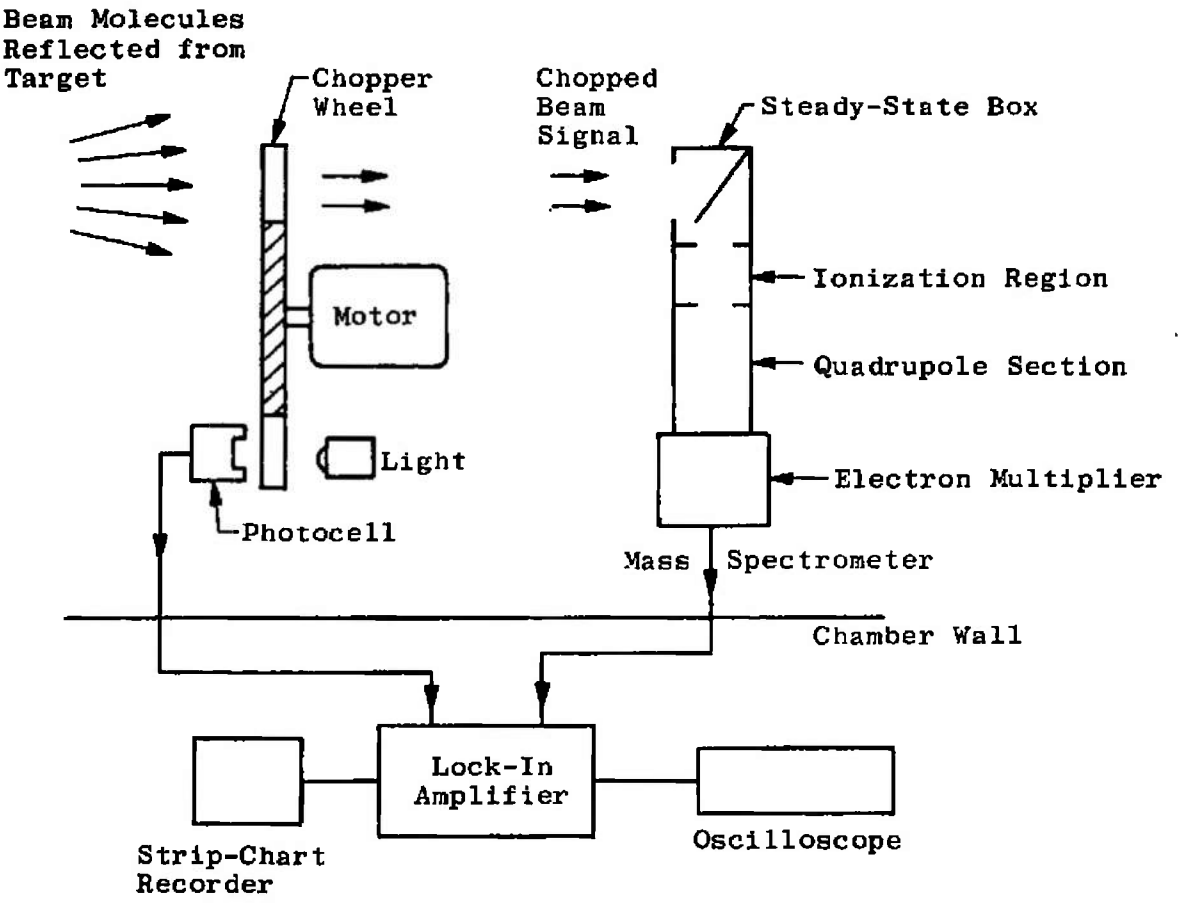

Fig. 7 Schematic Diagram of the Modulated Beam Detection System Used in Relative Cluster Abundances Measurements

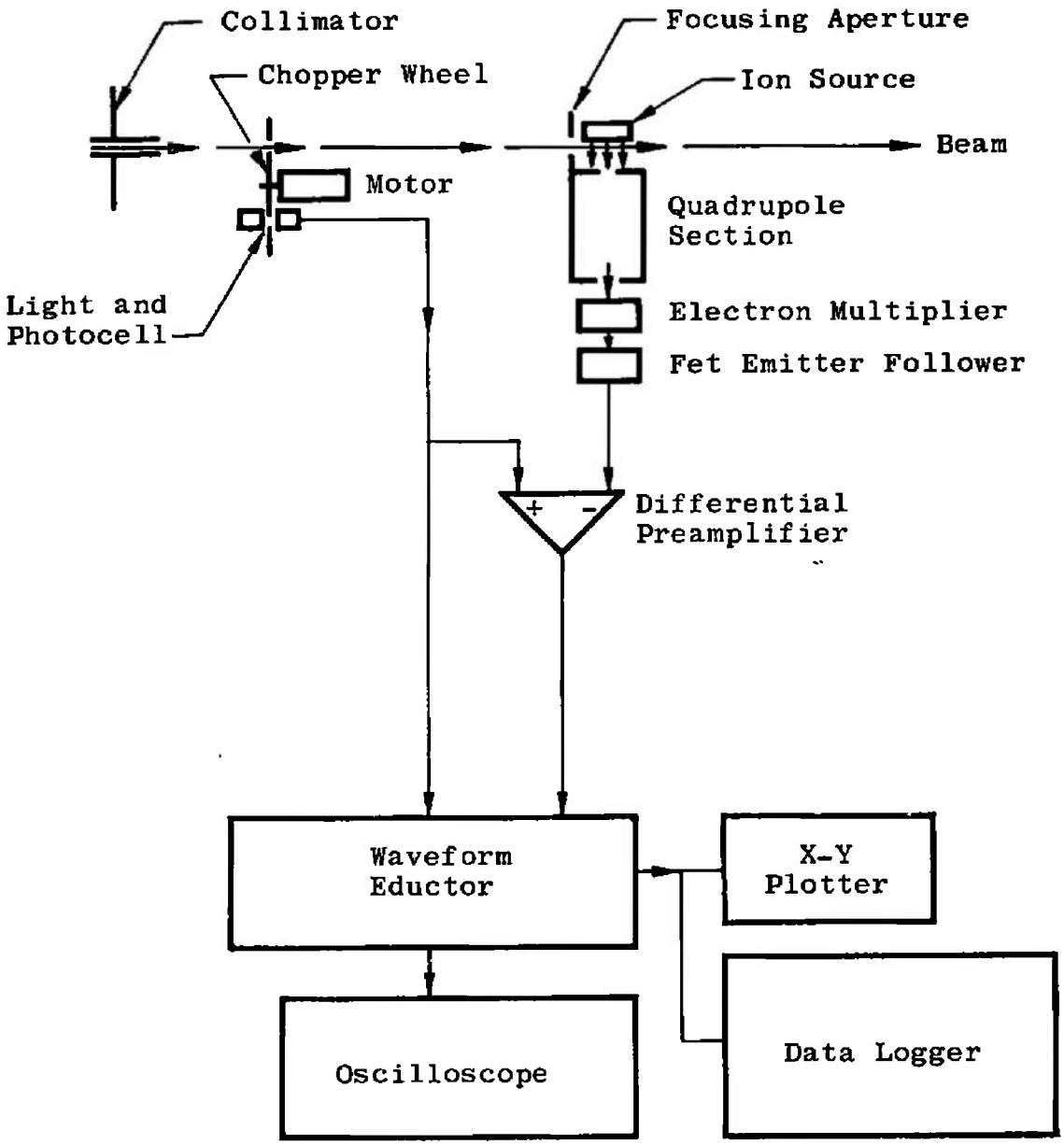

Fig. 8 Schematic Diagram of the Modulated Beam Detection Systems in the Time-of-Flight Measurements

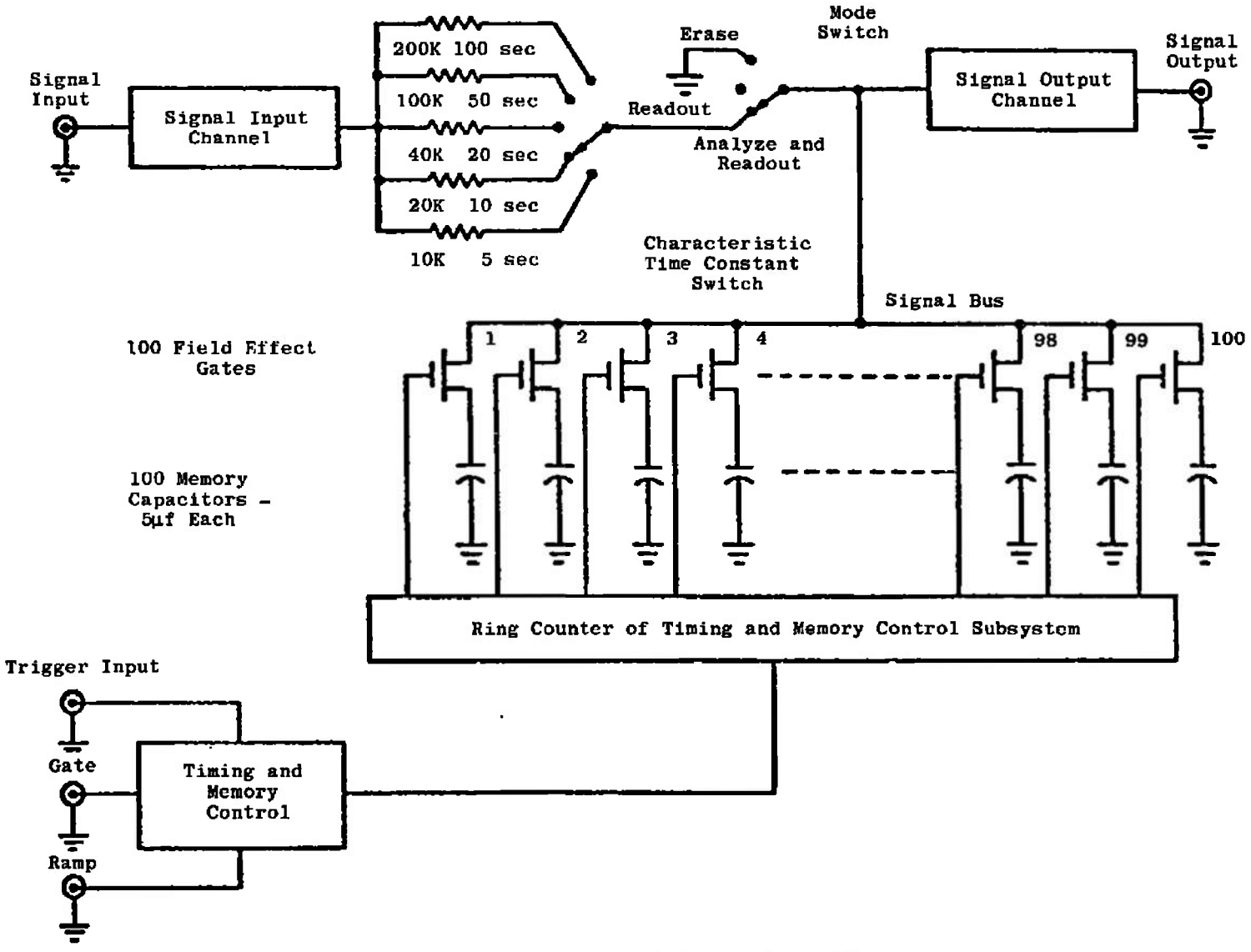

Fig. 9 Schematic Diagram of the Waveform Eductor

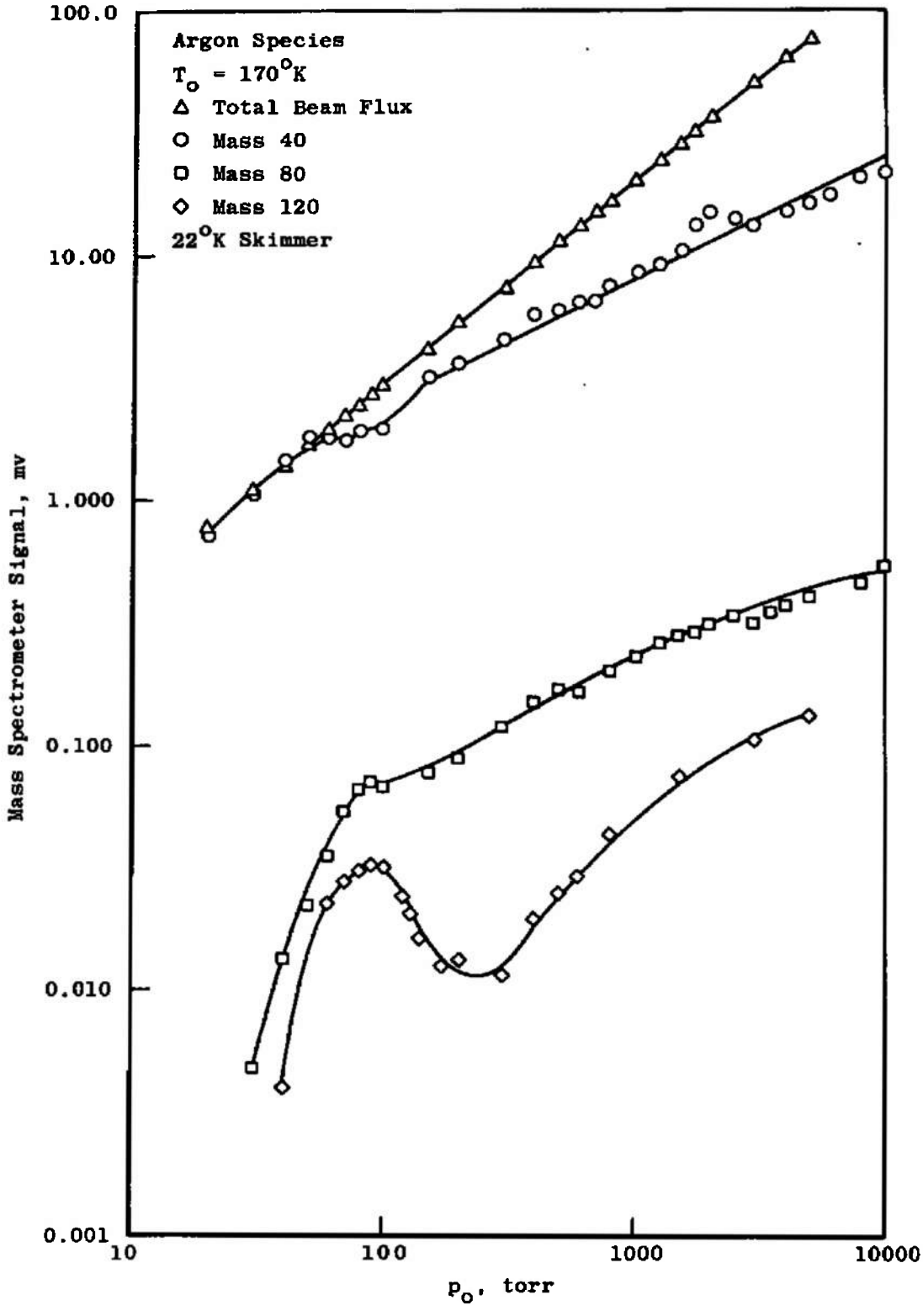

Fig. 10 Argon Cluster Concentrations, T_o = 170°K

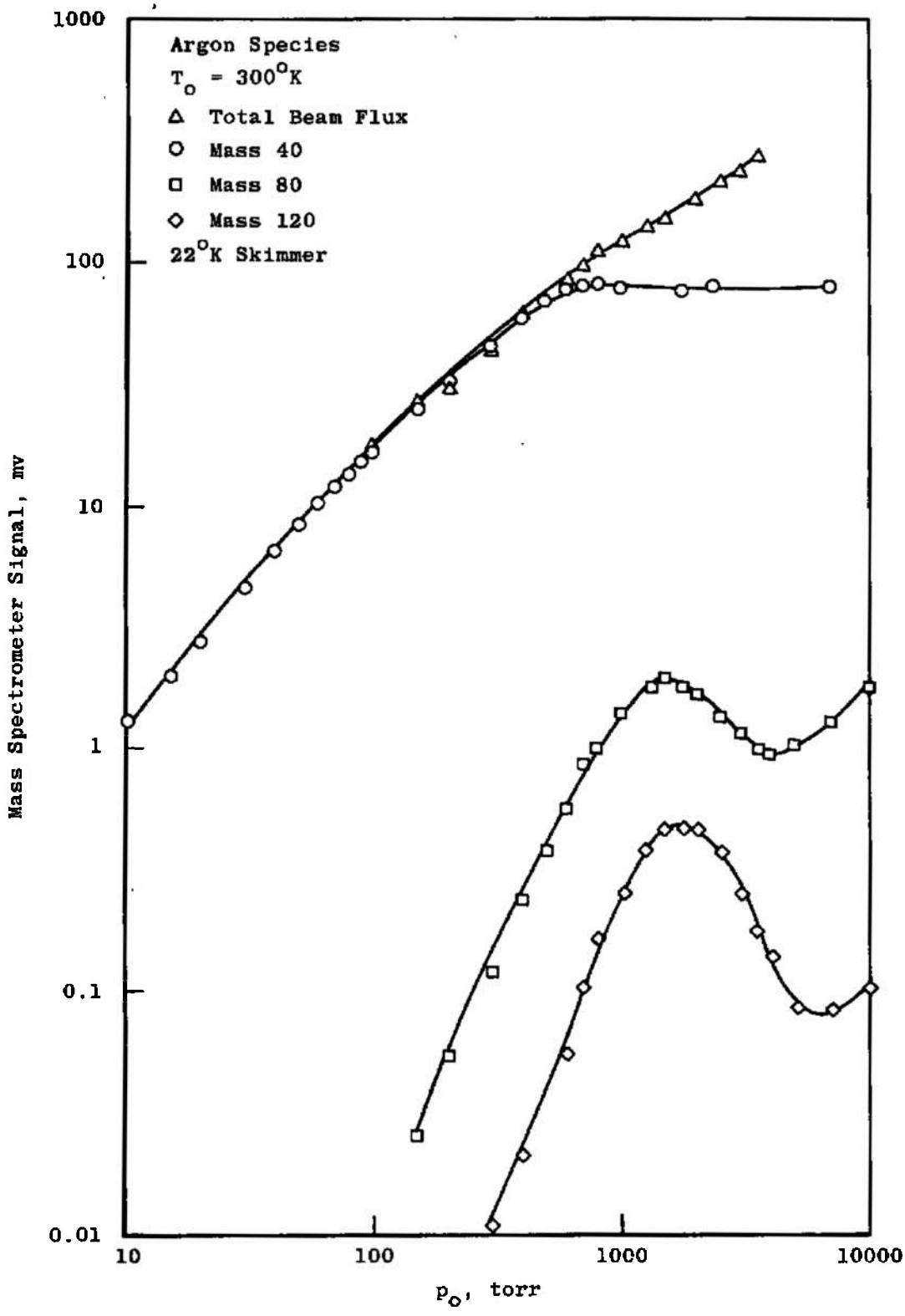

Fig. 11 Argon Cluster Concentrations, T_o = 300°K

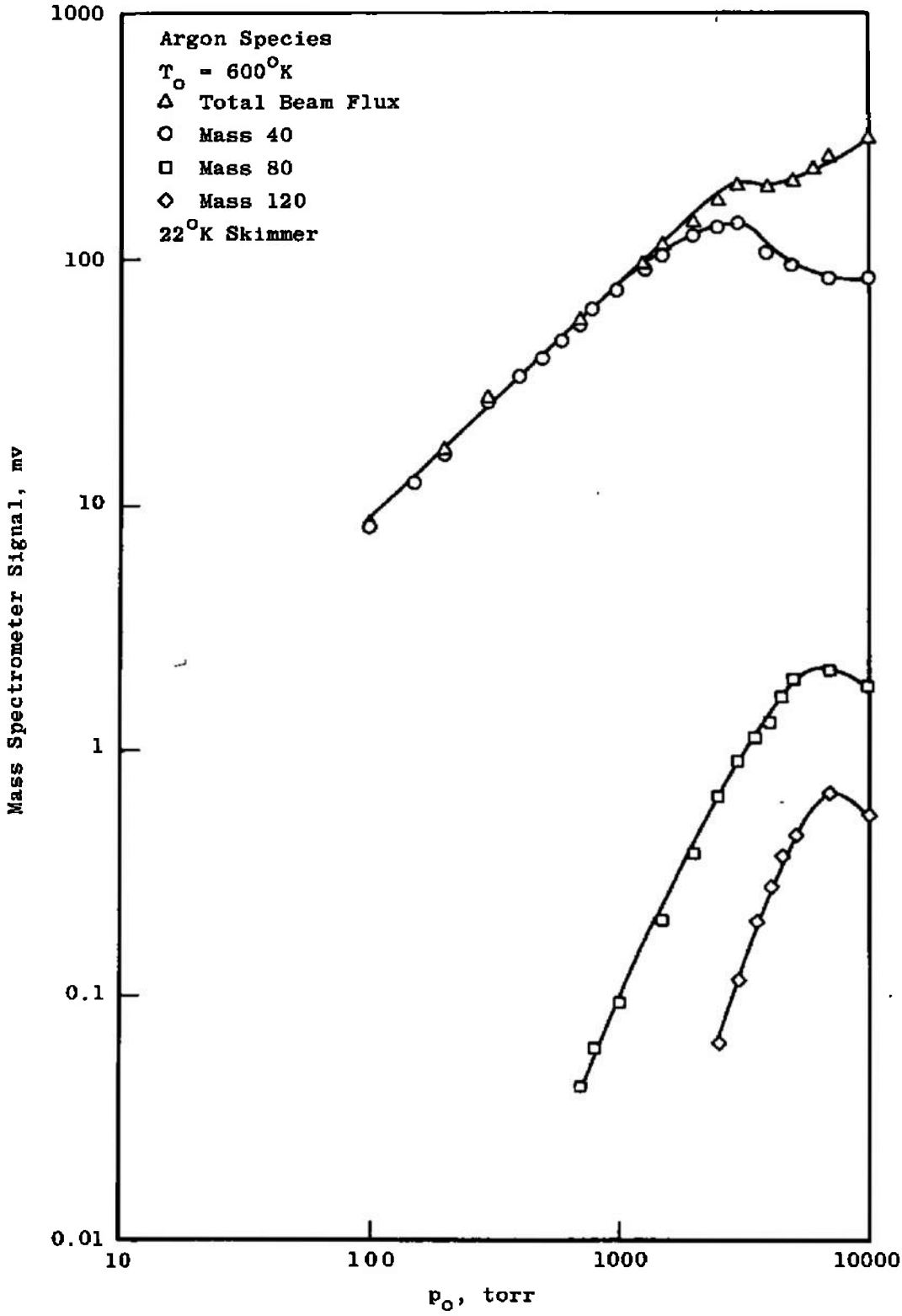

Fig. 12 Argon Cluster Concentrations, T_o = 600°K

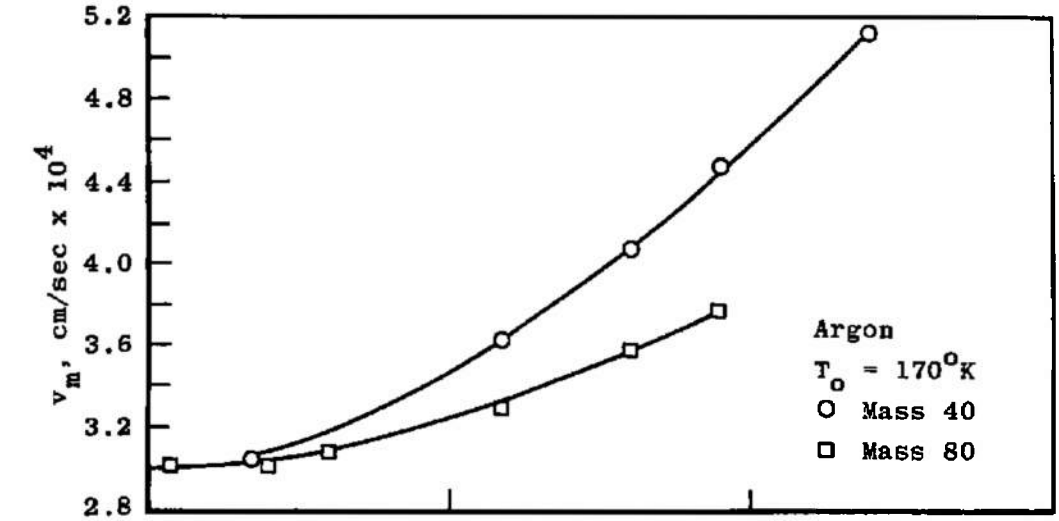

a. v_m versus p_o

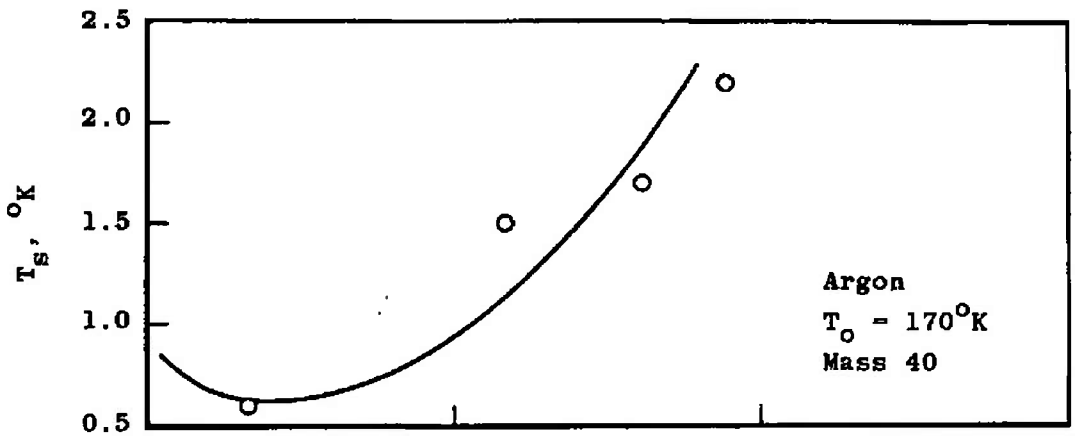

b. T_s versus p_o

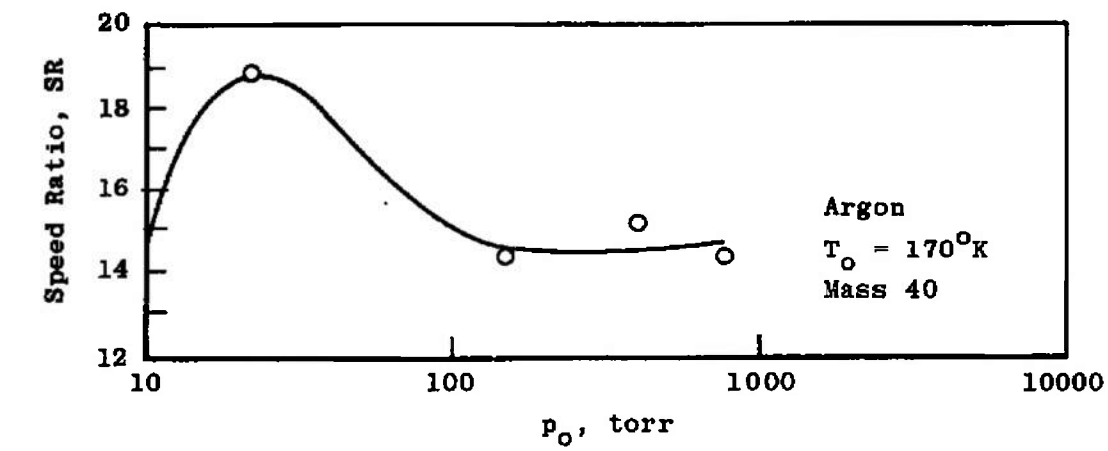

c. SR versus p_o

Fig. 13 Flow Field Properties, T_o = 170°K

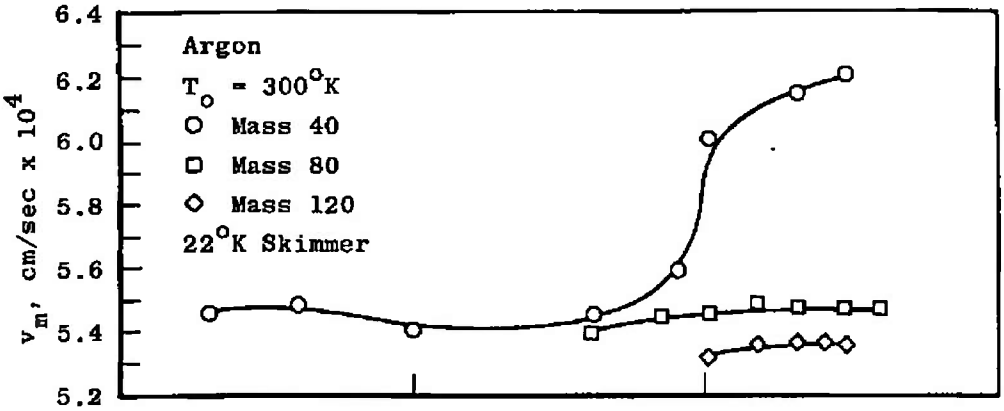

a. v_m versus p_o

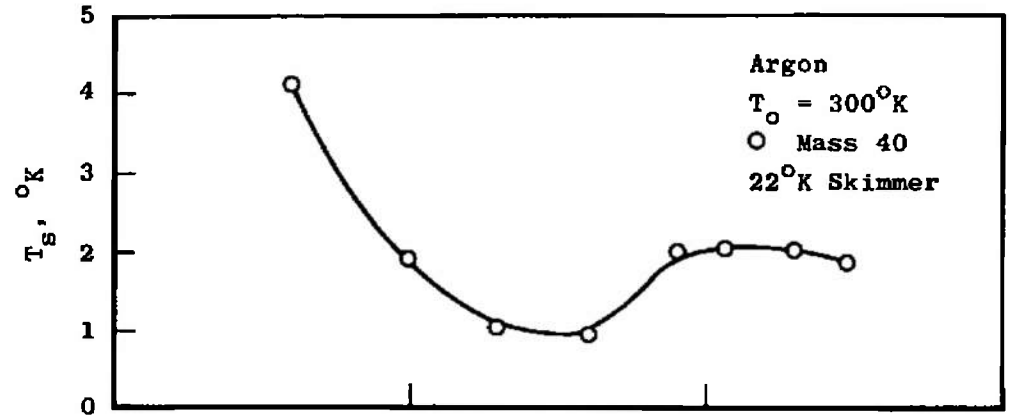

b. T_s versus p_o

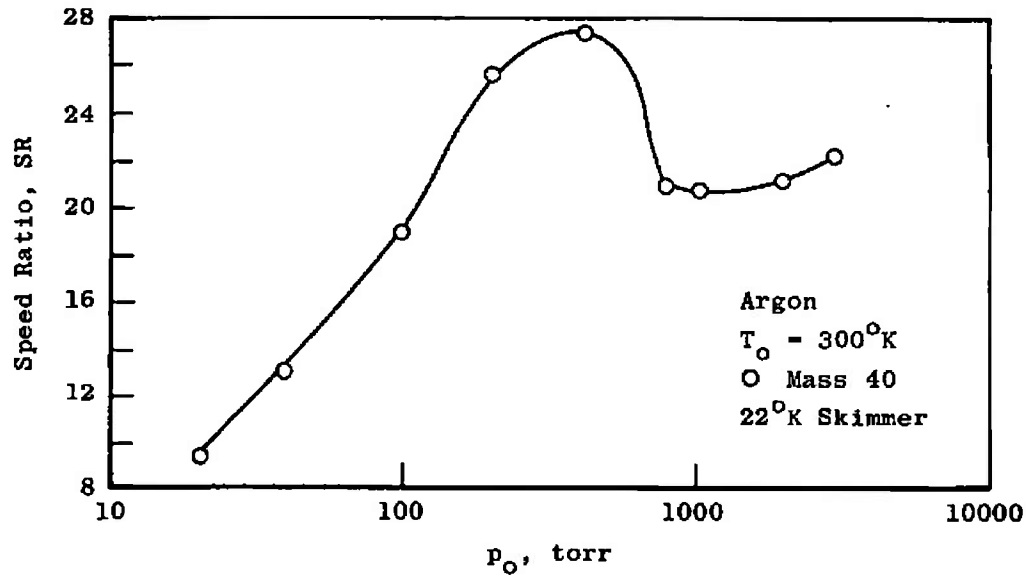

c. SR versus p_o

Fig. 14 Flow Field Properties, T_o = 300°K

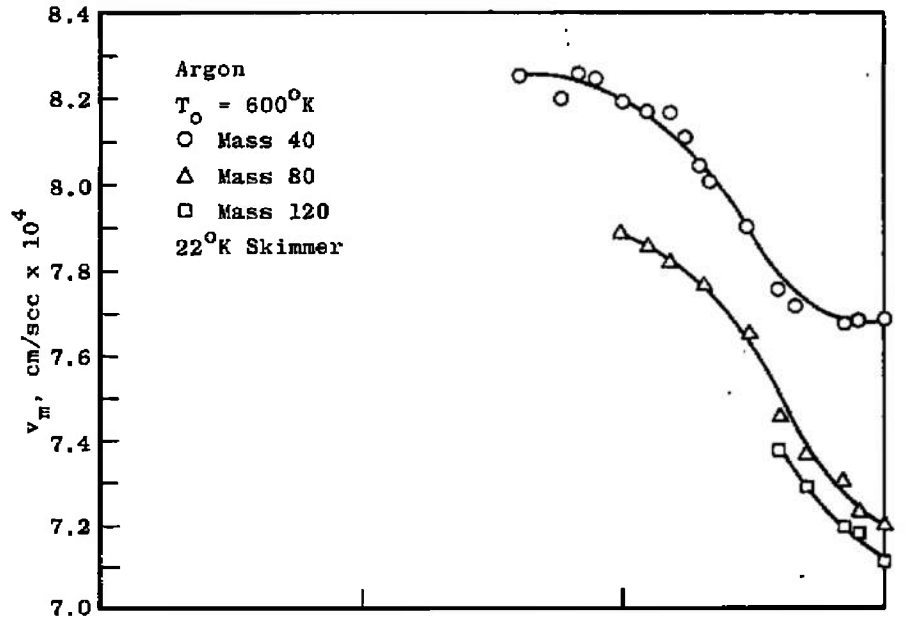

a. v_m versus p_o

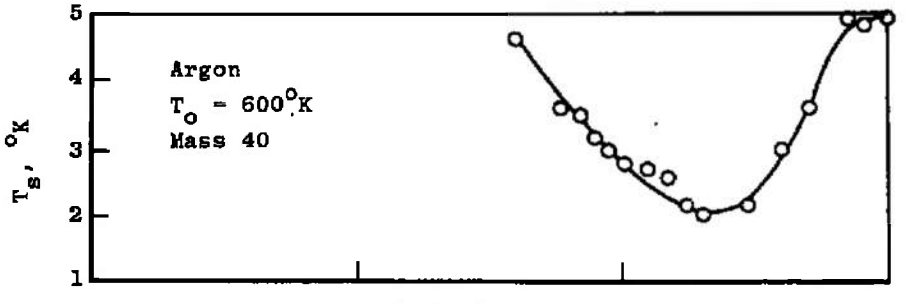

b. T_s versus p_o

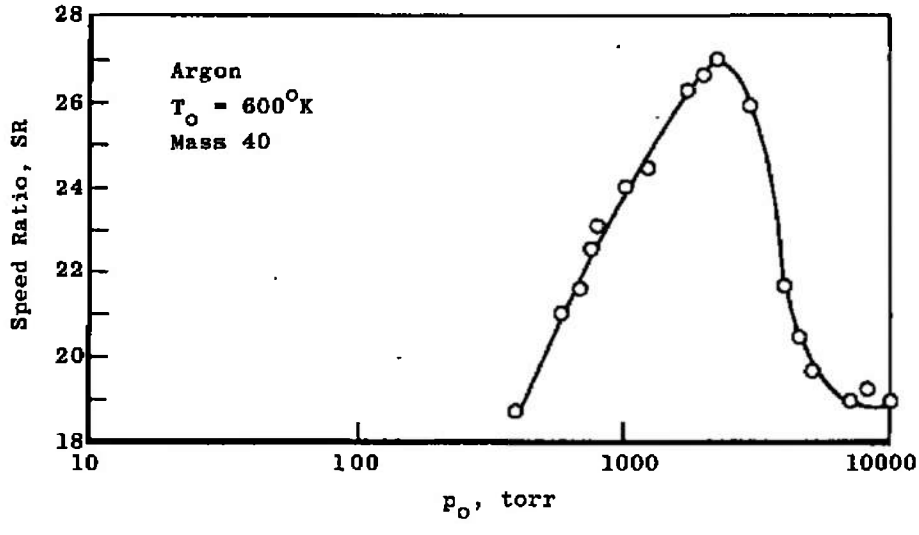

c. SR versus p_o

Fig. 15 Flow Field Properties, T_o = 600°K

APPENDIX II
THE SPEED RATIO

The speed ratio, SR, is a parameter used as a descriptive property of molecular beams in rarefied gas dynamics literature. It is defined as

$$SR = \frac{U_o}{\sqrt{2RT_s}} \tag{II-1}$$

In Eq. (II-1), U_o is the flow velocity of the beam, T is the static temperature, and R is the gas constant per unit mass.

Consider the denominator of the speed ratio

$$\sqrt{2RT_s} = \sqrt{2kT_s/m} = v_{mp} \tag{II-2}$$

where v_{mp} is the most probable velocity of a Maxwellian gas at temperature, T_s. The speed ratio, SR, can be thought of as a measure of how well the expansion process converts the random thermal velocity of the gas in the source into a flow velocity, U_o.

At the very low static temperatures associated with the free-jet expansion, the energy equation for a perfect gas

$$c_p T_o = c_p T_s + \frac{1}{2} m U_o^2 \tag{II-3}$$

closely approximates the condition

$$c_p T_o = \frac{1}{2} m U_o^2 \tag{II-4}$$

and

$$U_o = \sqrt{2c_p T_o/m} = \sqrt{[2\gamma/(\gamma - 1)]\, RT_o} \tag{II-5}$$

Normally, an increase in stagnation temperature, T_o, should always produce an increase in the speed ratio, SR. This relationship is drastically altered in a free-jet expansion. A few nozzle diameters downstream from the orifice the flow becomes free molecular, resulting in a "freezing" of both the Mach number and the temperature. This highest attainable Mach number is designated the terminal Mach number, M_T, and it is related to the speed ratio by Eq. (II-6):

$$SR = \frac{U_o}{\sqrt{2RT_s}} = \sqrt{\frac{\gamma}{2}}\ \frac{U_o}{\sqrt{\gamma RT_s}} = \sqrt{\gamma/2}\left(\frac{U_o}{a}\right) = \sqrt{\frac{\gamma}{2}}\, M_T \tag{II-6}$$

Note that

$$SR = SR\,(\gamma, M_T)$$

It is desired to measure the behavior of the various size molecular clusters throughout the flow field in terms of a single parameter. The values of γ appropriate for molecular clusters are unknown. If values for the clusters could be determined, γ could

still not be treated as a constant. The value of γ will change in the transition region between continuum and free molecular flow. The speed ratio, SR, provides a means of dealing with changes in M_T and γ for all size clusters throughout the flow field in terms of a single concept.

Additionally, Anderson, et al. (Ref 18), reasoned that the expansion process, which is governed by the stagnation conditions and the sonic orifice geometry, should be a function of the source Knudsen number, Kn_s. They were able to experimentally verify that argon gas follows the empirical relationship

$$M_T = Kn_s^{\frac{1-\gamma}{\gamma}} \tag{II-7}$$

where

$$Kn_s = \frac{\lambda_o}{D_n} \tag{II-8}$$

and D_n is the orifice diameter and λ_o is the mean-free path of the gas in the source at stagnation conditions. This relationship is valid over the entire range of source conditions reported in this study.

Empirically then, the speed ratio, can be linked to source conditions by the following development:

$$SR = \sqrt{\frac{\gamma}{2}}\ M_T = \sqrt{\frac{\gamma}{2}}\ Kn_s^{\frac{1-\gamma}{\gamma}} \tag{II-9}$$

$$\lambda = \frac{1}{\sqrt{2}}\ \frac{1}{4\pi r^2 n} = \frac{1}{\sqrt{2}}\ \frac{kT_o}{4\pi r^2 p_o} \tag{II-10}$$

$$SR = \sqrt{\frac{\gamma}{2}} \left\{ \frac{1}{D_n}\ \frac{1}{\sqrt{2}}\ \frac{kT_o}{4\pi r^2 p_o} \right\}^{\frac{1-\gamma}{\gamma}} \tag{II-11}$$

$$SR \propto \frac{1}{(T_o)^{0.4}} \qquad \text{(constant } p_o\text{)} \tag{II-12}$$

and SR will decrease as T_o increases.

To summarize the development thus far, it can be said that the speed ratio is a descriptive property of a molecular beam which can be related by valid empirical data to the source conditions if argon is used as the test gas.

Security Classification

DOCUMENT CONTROL DATA - R & D

(Security classification of title, body of abstract and indexing annotation must be entered when the overall report is classified)

1. ORIGINATING ACTIVITY (Corporate author)
Arnold Engineering Development Center, ARO, Inc., Operating Contractor, Arnold Air Force Station, Tennessee 37389

2a. REPORT SECURITY CLASSIFICATION
UNCLASSIFIED

2b. GROUP
N/A

3. REPORT TITLE

THE EFFECTS OF CONDENSATION ON THE FLOW FIELD PROPERTIES IN FREE-JET EXPANSIONS OF ARGON

4. DESCRIPTIVE NOTES (Type of report and inclusive dates)
July 1969 to April 1970 - Final Report

5. AUTHOR(S) (First name, middle initial, last name)
E. C. Ruby, R. F. Brown, and M. R. Busby, ARO, Inc.

6. REPORT DATE	7a. TOTAL NO. OF PAGES	7b. NO. OF REFS
August 1970	49	18

8a. CONTRACT OR GRANT NO.	9a. ORIGINATOR'S REPORT NUMBER(S)
F40600-71-C-0002	
b. Program Elements 64719F and 62101F	AEDC-TR-70-142
c.	9b. OTHER REPORT NO(S) (Any other numbers that may be assigned this report)
d.	ARO-VKF-TR-70-142

10. DISTRIBUTION STATEMENT
This document has been approved for public release and sale; its distribution is unlimited.

11. SUPPLEMENTARY NOTES	12. SPONSORING MILITARY ACTIVITY
Available in DDC.	AEDC, AFSC, Arnold Air Force Station, Tenn. 37389 and AFCRL, L. G. Hanscom Field, Bedford, Mass. 01730

13. ABSTRACT

Molecular beam techniques and a time-of-flight velocity distribution detector system were used to investigate the effects of condensation in free-jet expansions of argon. A 1-in.-diam skimmer cooled to 22°K was used to eliminate skimmer interaction. The data reported are for 170, 300, and 600°K argon expanded into a vacuum from source pressures of from 10 to 10,000 torr and with a nozzle-skimmer separation distance of 650 nozzle diameters. The data revealed that the terminal velocity of the monomer species can be greater than predicted by $c_p T_o = 1/2mv_m^2$ when condensation occurs. This is hypothesized to be the result of the heat of condensation being added to the flow field. Also, when condensation occurs, the static temperature increases. Terminal speed ratios as high as 27.5 were measured during these tests.

DD FORM 1 NOV 65 1473

UNCLASSIFIED
Security Classification

14. KEY WORDS	LINK A ROLE	LINK A WT	LINK B ROLE	LINK B WT	LINK C ROLE	LINK C WT
condensation						
flow fixed properties						
free-jet expansion of argon --						
aerodynamic molecular beam techniques						
velocity distribution detector system						
molecular cluster formation						

1. Argon -- Condensation